

1
2
3
4
5
6
7
8
9
10
11
12
13
14
15
16
17
18
19
20
21
22
23
24
25
26
27
28
29
30
31
32
33
34
35
36
37
38
39
40
41
42
43
44
45
46
47

Coastal Sea Level rise at Senetosa (Corsica) during the Jason altimetry missions

Yvan Gouzenes¹, Fabien Léger¹, Anny Cazenave^{1,2}, Florence Birol¹, Pascal Bonnefond³,
Marcello Passaro⁴, Fernando Nino¹, Rafael Almar¹, Olivier Laurain⁵, Christian Schwatke⁴,
Jean-François Legeais⁶ and Jérôme Benveniste⁷

1. LEGOS, Toulouse; 2. ISSI, Bern; 3. Observatoire de Paris-SYRTE, Paris ; 4. TUM,
Munich; 5. Observatoire de la Côte d'Azur-Géoazur, Sophia-Antipolis; 6. CLS, Ramonville
St Agne; 7. ESA-ESRIN, Frascati.

Final Version
14 August 2020

Corresponding author: Anny Cazenave (anny.cazenave@legos.obs-mip.fr)

48
49
50
51

52 **Abstract**

53 In the context of the ESA Climate Change Initiative project, we are engaged in a regional
54 reprocessing of high-resolution (20 Hz) altimetry data of the classical missions in a number of
55 world's coastal zones. It is done using the ALES (Adaptive Leading Edge Subwaveform)
56 retracker combined with the X-TRACK system dedicated to improve geophysical corrections
57 at the coast. Using the Jason-1&2 satellite data, high-resolution, along-track sea level time
58 series have been generated and coastal sea level trends have been computed over a 14-year
59 time span (from July 2002 to June 2016). In this paper, we focus on a particular coastal site
60 where the Jason track crosses land, Senetosa, located south of Corsica in the Mediterranean
61 Sea, for two reasons: (1) the rate of sea level rise estimated in this project increases significantly
62 in the last 4-5 km to the coast, compared to what is observed further offshore, and (2)
63 Senetosa is the calibration site for the Topex/Poseidon and Jason altimetry missions,
64 equipped for that purpose with in situ instrumentation, in particular tide gauges and GNSS
65 antennas. A careful examination of all the potential errors that could explain the increased
66 rate of sea level rise close to the coast (e.g., spurious trends in the geophysical corrections,
67 imperfect intermission bias estimate, decrease of valid data close to the coast and errors in
68 waveform retracking) has been carried out, but none of these effects appear able to explain
69 the trend increase. We further explored the possibility it results from real physical processes.
70 Change in wave conditions was investigated but wave set up was excluded as a potential
71 contributor because of too small magnitude and too localized in the immediate vicinity of
72 the shoreline. Preliminary model-based investigation about the contribution of coastal currents
73 indicates that it could be a plausible explanation of the observed change in sea level trend
74 close to the coast.

75

76 **1. Introduction**

77 Since the early 1990s, satellite altimetry provides invaluable observations of the global mean
78 sea level and its regional variability. In the recent years, this data set has generated an
79 abundant literature on the processes causing sea level change at global and regional scales, as
80 well as on closure of the sea level budget (e.g., Church et al., 2013, Stammer et al., 2013,
81 Dieng et al., 2017, Nerem et al., 2018, WCRP, 2018, SROCC, 2019). In addition to the global
82 mean rise and superimposed regional trends, changes in small scale processes such as local
83 atmospheric effects, baroclinic instabilities, coastal trapped waves, shelf currents, waves,
84 fresh water input from rivers in estuaries, can substantially modify the rate of sea level change
85 at the coast compared to open sea regions (Woodworth et al., 2019, Melet et al., 2018,
86 Piecuch et al., 2018, Dodet et al., 2019, Durand et al., 2019). In addition, ground subsidence
87 may amplify the rate of sea level change at the coast (Woppelmann and Marcos, 2016). In
88 terms of societal impacts, what really matters in the coastal zone is indeed the sum of the
89 global mean sea level rise plus the regional trends and the local processes.

90 Up to recently, due to land contamination of radar echoes and less precise geophysical
91 corrections, classical altimetry did not provide reliable sea level data in a band of 10-15 km
92 along coastlines. However different studies have shown that using adapted reprocessing of
93 altimetry measurements and improving geophysical corrections allows retrieving a large
94 amount of valid sea level close to the coast (e.g., Cipollini et al., 2018, Passaro et al., 2015,
95 Marti et al., 2019). In addition, despite having a much higher noise level than the classical 1
96 Hz altimetry data, high-resolution 20 Hz measurements allow to recover more information on
97 coastal sea level variations (Birol and Delebecque, 2014, Leger et al., 2019).

98 In the context of the Climate Change Initiative (CCI) project of the European Space
99 Agency (ESA), we have initiated a reprocessing of high-resolution (20 Hz) altimetry data of
100 the Jason-1 and Jason-2 missions along coastal zones of Western Africa, Northern Europe and
101 Mediterranean Sea. The ALES (Adaptive Leading Edge Subwaveform) retracker (Passaro et
102 al., 2014) was applied to estimate the satellite-sea surface distance (called range) which was
103 further combined with the X-TRACK processing chain dedicated to improve geophysical
104 corrections at the coast (Birol et al., 2017). This allowed us to derive along-track sea level
105 anomaly (SLA) time series (Leger et al., 2019) from which coastal sea level trends were
106 estimated. Results show that in a number of sites, coastal sea level rates computed over a 14-
107 year time span (2002-2016) significantly deviate from the open ocean rate within 5 km to the
108 coast (Marti et al., 2019).

109

110 In the present study, we focus on a particular site, Senetosa, located southern Corsica in the
 111 Mediterranean Sea (41° 33'N, 8°48'E), for two reasons: (1) in this region, the computed rate
 112 of sea level rise increases significantly in the last 3-5 km to the coast, and (2) there is a
 113 Jason satellite track that crosses land at Senetosa, a calibration site for altimetry missions
 114 chosen since the launch of the Topex/Poseidon mission in 1992 and equipped for that purpose
 115 with in situ instrumentation, in particular tide gauges and GNSS antennas (Bonfond et al.,
 116 2019). This calibration site provides an independent reference to explore the near-shelf signal
 117 observed in altimetry data.

118

119 **2. Data and method**

120 As presented in detail in Marti et al. (2019) and Léger et al. (2019), here we use the regional
 121 X-TRACK/ALES along-track 20 Hz SLA data derived from Jason-1 and Jason-2 missions
 122 (DOI: 10.5270/esa-sl_cci-xtrack_ales_sla-200201_201610-v1.0-201910). This product is
 123 based on new ranges and new sea state bias corrections estimated using the ALES retracker
 124 (see details on the retracking methodology in Passaro et al., 2014), and further combined with
 125 the X-TRACK software developed at CTOH (Center of Topography of the Ocean and the
 126 Hydrosphere) at LEGOS (Laboratoire d'Études en Géophysique et Océanographie Spatiales).
 127 The new X-TRACK/ALES processing system first downloads from the altimetry database
 128 hosted by the French National Observations Service for altimetry called CTOH
 129 (<http://ctoh.legos.obs-mip.fr/>), all parameters needed to compute the sea level anomaly (orbit
 130 solution, altimeter ranges, instrumental, environmental and geophysical corrections). These
 131 parameters come from the Geophysical Data Records (GDRs) data sets distributed by the space
 132 agencies for the different altimetry missions. ALES range and SSB products come from TUM.
 133 Additional geophysical corrections are provided by the RADS altimeter database
 134 (<http://rads.tudelft.nl/rads/rads.shtml>) and the University of Porto (for the GPD+ wet
 135 tropospheric correction, Fernandes et al., 2015). Concerning the geophysical corrections, we
 136 used the standards defined in the ESA CCI sea level project (<http://www.esa-sealevel-cci.org/>).
 137 These are summarized in Table 1.

138

Parameter	Source	Jason-1 / Jason-2
Altitude	GDR	Altitude of satellite
Range	ALES/TUM	20 Hz Ku band ALES corrected altimeter range (Passaro et al. 2014)

Sigma0	ALES/TUM	20 Hz Ku band ALES altimeter sigma0 (Passaro et al. 2014)
Ionosphere	GDR	From dual-frequency altimeter range measurement
Dry troposphere	GDR	From ECMWF model
Wet troposphere	University of Porto	GPD+ correction (Fernandes et al. 2015)
Sea-state bias	ALES/TUM	Sea-state bias correction in Ku band, ALES retracking (Passaro et al. 2018)
Solid tides	RADS	From tide potential model (Cartwright and Taylor 1971, Cartwright and Eden 1973)
Pole tides	GDR	From Wahr 1985
Loading effect	RADS	From FES 2014 (Carrere et al. 2012)
Atmospheric correction	RADS	From MOG2D-G (Carrere and Lyard 2003) + inverse barometer
Ocean tide	RADS	From FES 2014 (Carrere et al. 2012)

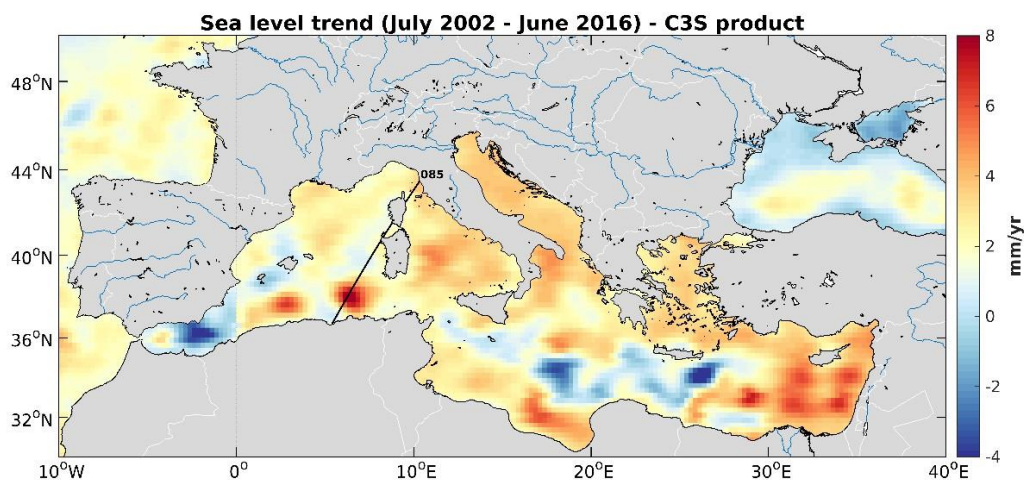
139

140 *Table 1. List of altimetry parameters and geophysical corrections used in the computation of the*
141 *coastal sea level products.*

142

143 A dedicated editing strategy was further applied to eliminate noisy data. For each orbit cycle, the
144 temporal behavior of each geophysical correction was analyzed along the satellite track. Abrupt
145 changes were considered as spurious and removed (Birol et al., 2017). This strategy has proved to
146 be very efficient in recovering a significant amount of valid altimeter measurements that were
147 otherwise flagged in the standard GDR products (Jebri et al., 2016). In a second step, all corrections
148 were recomputed at the 20-Hz high-rate using only the valid data, through interpolation/extrapolation
149 method. The sea level data of each cycle were further projected onto fixed points along a nominal
150 ground track and converted into SLAs by subtracting a reference mean sea surface. At this stage of
151 the processing, a regional dataset of SLA time series with a spatio-temporal resolution of 10 days
152 and 20Hz (~0.3 km) was produced for each Jason mission. To obtain a single multi-mission product,
153 an inter-mission bias was estimated and removed. This was done at regional level by computing the

154 mean sea level differences between the two missions over their overlapping period (calibration
155 phase). The resulting SLAs were further averaged on a monthly basis at every 20 Hz point and an
156 additional editing was performed to remove outliers (details in Marti et al., 2019).
157 In this study we focus on the section of Jason track 85 located off the southwestern coast of
158 Corsica island (western Mediterranean Sea) (see Fig. 1).
159



160

161

162 *Fig. 1. Location of the Jason track 85 crossing Corsica at the Senetosa site (black straight line).*
163 *The background maps shows sea level trends over 2002-2016, based on gridded altimetry data*
164 *from the Copernicus Climate Change Service (C3S; <https://climate.copernicus.eu/sea-level>)*

3. The Senetosa calibration site

165 Since 1998, a calibration site of the Topex/Poseidon and Jason missions has
 166 operated near the Senetosa lighthouse with support from CNES (Centre National
 167 d'Études Spatiales, France), NASA (National Aeronautics and Space Administration, USA)
 168 and the Observatoire de la Côte d'Azur (France). It is equipped with different in situ
 169 instrumentation, including weather stations, several tide gauges and GNSS antenna. Since
 170 1998, this calibration site has been widely used to validate the altimetry-based sea surface
 171 height data (Bonfond et al., 2003a,b, 2010, 2011). Fig.2 is a Google Earth image of the
 172 coast, showing the geographical configuration of the Senetosa calibration site, with the
 173 location of the tide gauges, the GNSS antenna and the Jason track. Three tide gauges were
 174 operating during our study period (M3, M4 and M5). M4 and M5, a few tens of cm apart,
 175 are located on the western part of the coastline sheltered from northwestward wind
 176 forcing. M3 at 1.7 km eastward of M4/M5 is more exposed to open sea conditions from the
 177 west.

178
 179 Vertical land motion time series are available from the GNSS reference receiver located close
 180 to the lighthouse (G0 reference marker in Fig.2). The tide gauges have been regularly leveled
 181 relatively to the G0 reference marker with no relative motion detected so far at the millimeter
 182 level over 10 years. Trends in sea level and vertical land motions derived from these
 183 instruments at Senetosa are discussed in section 5.

184



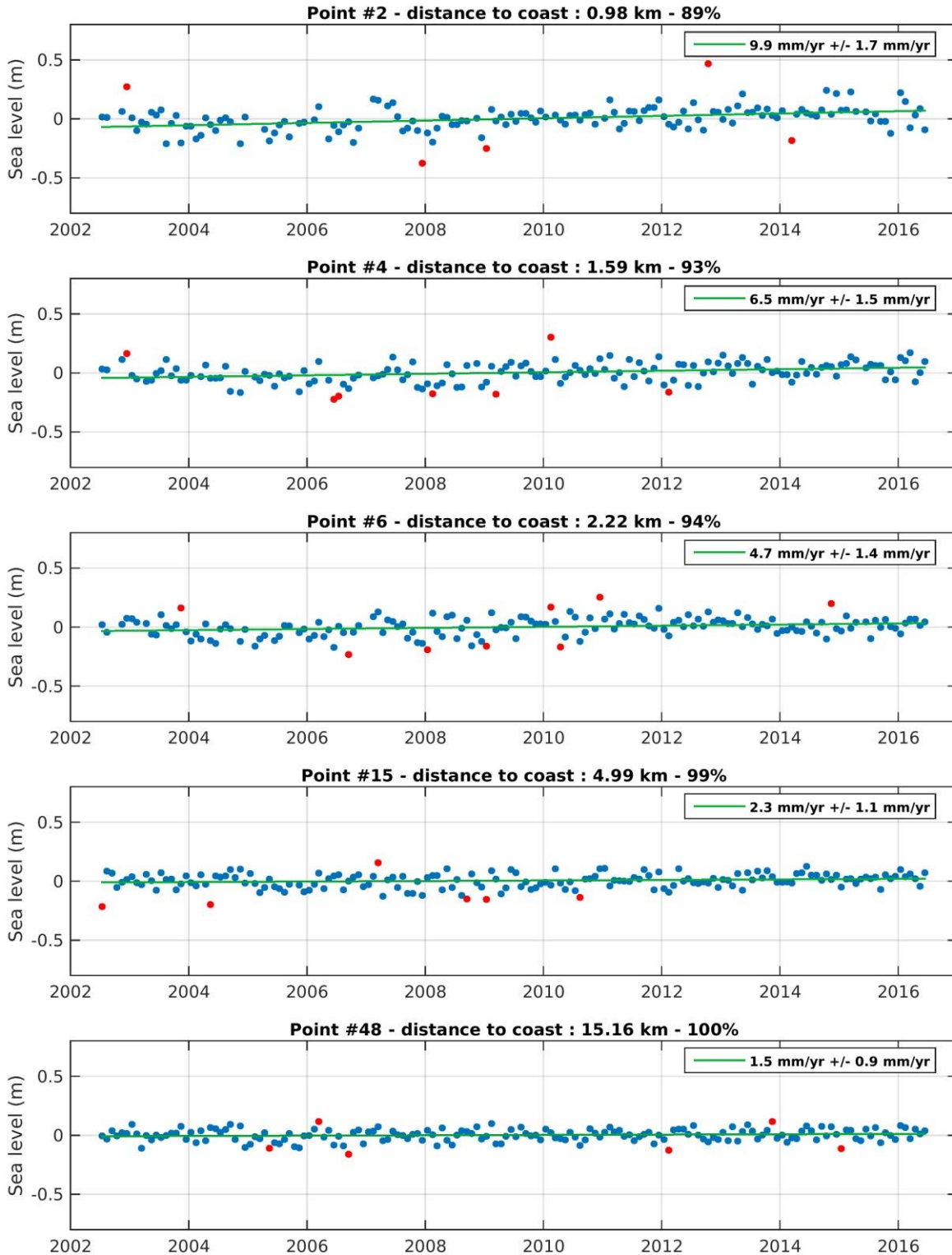
186
187 *Fig. 2. Google Earth image of the Senetosa calibration site. The two tide gauge sites (referred*
188 *as M4/M5 and M3) are shown by the red dots. The G0 reference marker (G0) is indicated by a*
189 *white square and the Jason ground track by the white straight line.*

190
191

192 **4. Analysis of the coastal sea level trends off Senetosa**

193 **4.1 Coastal sea level trends derived from altimetry data**

194 Following the data processing described above, we focus on monthly SLA time series sampled
195 at 20 Hz (~350 m in the along-track direction), from 15 km offshore to the coastline. Examples
196 of along-track SLA time series at coastal points, located at 1 km, 1.6 km, 2.2 km, 5 km and
197 15 km from the coast respectively, are shown in Fig.3.



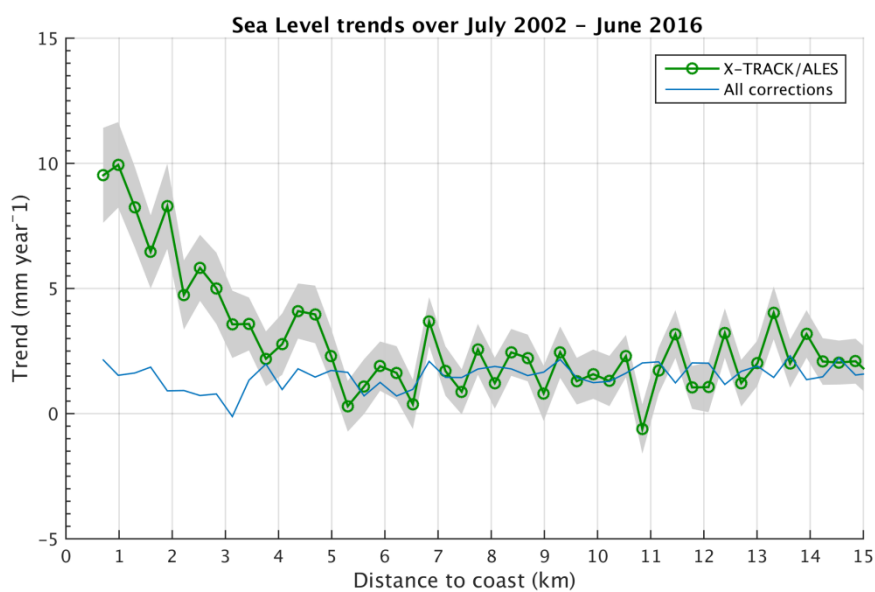
200
201
202

203 *Fig. 3. Examples of sea level anomalies time series for 20-Hz points located at different*
 204 *distances from the coast. The distance to coast, percentage of valid data and sea level trends*
 205 *are indicated on each plot. The green curve is the regression line adjusted to the data. The*
 206 *red points on the time series correspond to outliers detected using a simple 2-sigma filter*
 207 *(sigma corresponding to the SLA standard deviation). These are not considered to compute*
 208 *the regression line.*

209
210
211
212

213 For each 20 Hz point, we have then computed the regression line of the resulting SLA time
214 series and the associated standard deviation (1-sigma) based on the least squares fit, to estimate
215 sea level trends over the study time span. Corresponding along track sea level trends against
216 distance to the coast (from 15 km offshore) are shown in Fig.4.

217
218
219
220
221
222
223
224
225
226
227
228
229
230
231
232
233
234
235
236
237



238

239 *Fig. 4. ltimetry-based sea level trends over July 2002-June 2016 around Senetosa against*
240 *distance to the coast. Shaded area corresponds to trend uncertainty range. The light blue*
241 *curve is the sum of trends in individual corrections.*

242

243 As shown in Fig.4, beyond ~ 5 km from the coast towards the open sea, the trend over 2002-
244 2016 is relatively stable and on average on the order of 2-3 mm/yr. High frequency
245 oscillations around this value are observed between adjacent points but these are likely due to
246 noise and we note they are of the same order of magnitude or only slightly larger than the
247 standard deviation of trend estimates at each point (of ~1.5 mm/yr).

248 As also shown in Fig.4, we note an almost continuous increase in the trend in the last ~4-5 km
249 to coast. The corresponding trend uncertainties (standard deviation) are not significantly
250 larger than offshore (<2 mm/yr).

251

252 4.2 Robustness of the computed coastal trends

253 In coastal areas, precision of sea surface height from altimetry is limited by inaccuracies in
 254 some of the applied geophysical corrections (including sea-state bias, wet tropospheric
 255 correction, dynamical atmospheric correction and ocean tides) and from the distorted shape of
 256 the radar waveforms as the satellite approaches land (Vignudelli et al., 2011 and Cipollini et al.,
 257 2018).

258 The corresponding altimetry measurements are often discarded by the processing chains or
 259 flagged in the data sets as potentially erroneous, leading to low confidence sea level
 260 trend estimates near the coastline. These estimates can also be impacted by the lower
 261 percentage of valid data in the coastal zone, as well as by the uncertainty in the bias estimate
 262 between the two successive missions Jason-1 and Jason-2. In order to check whether the sea
 263 level trend increase close to the coast reported in section 4.1 is associated to one of these
 264 factors, each of them is independently examined.

265

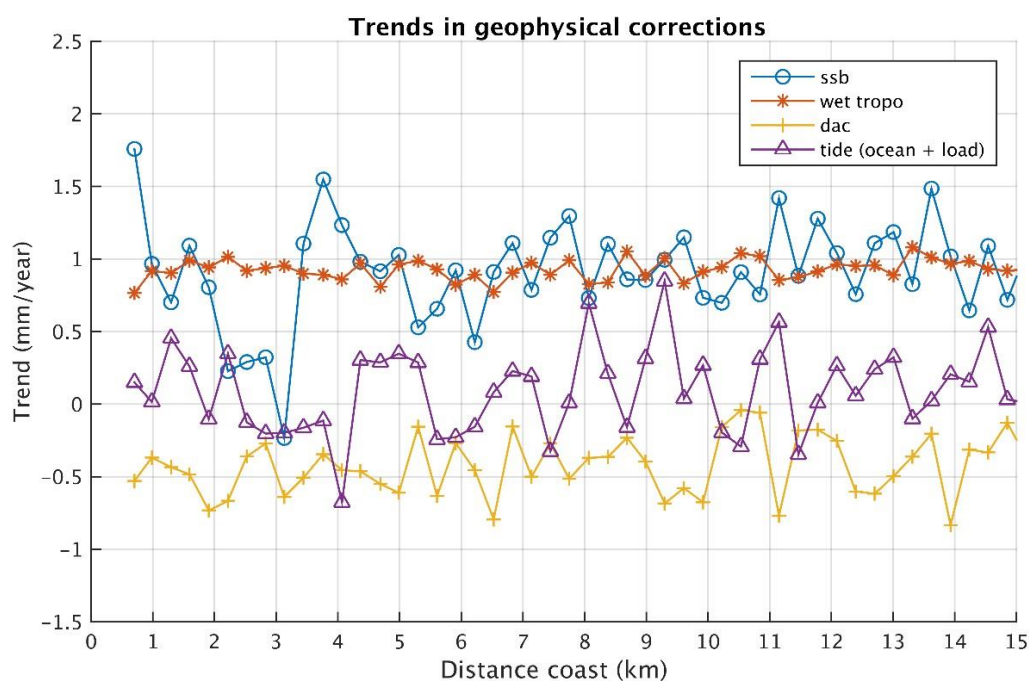
266 4.2.1 Coastal errors in the geophysical corrections

267 We first computed and plotted the geophysical correction trends against distance to the coast
 268 for the sea-state bias (ssb), wet atmospheric correction, atmospheric loading (called DAC-
 269 dynamic atmospheric correction-) and ocean and loading tide correction (Fig.5).

270

271

272



273

274
275

276 *Fig. 5. Trends in the geophysical corrections (sea state bias/ssb, wet tropospheric correction,*
277 *dynamic atmospheric correction/dac, ocean tide plus ocean loading tide) as a function of*
278 *distance to coast. Note that the vertical scale is different from Fig.4.*

279

280 Trends in the geophysical corrections are rather small and their amplitude in the range +/- 1
281 mm/yr, except for the ssb that shows a larger trend within 4 km to coast, but always less than
282 2 mm/yr. It is worth mentioning that the ssb is a function of significant wave height (SWH)
283 and backscatter coefficient (both related to wind speed). In the ALES retracking the ssb is
284 recomputed for each 20-Hz point. So a trend in ssb may be due to either a different behavior
285 of the SWH and wind speed at the coast, or to changes in backscatter properties.

286 The sum of these geophysical correction trends is plotted in Fig.4 (blue line). Even if the
287 geophysical corrections, and especially the ssb, are more uncertain close to the coast, Fig. 4
288 suggests that the continuous increase in the sea level trends observed in the last ~4 km to the
289 coast may not be due to trends in the geophysical corrections. It remains that the empirical
290 formulation used for the ssb correction may not be valid close to the coast where waves could
291 have a different behavior compared to the open sea. This will be discussed in section 6.1.

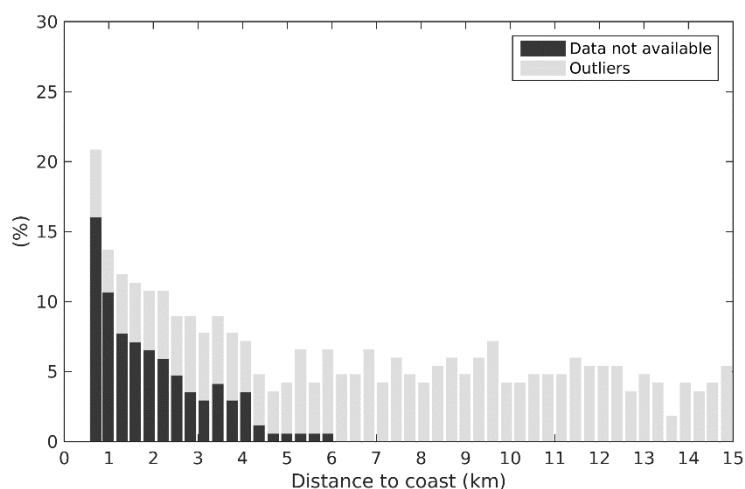
292

293 *4.2.2 Coastal changes in the percentage of valid data*

294 We next examined the possible impact on the trend estimation of the decrease in valid data in
295 the last 3-4 km to coast. The original percentage of valid data at each 20-Hz point decreases
296 with distance to the coast, as shown in Fig.6. We resampled the along-track sea-level records
297 keeping only the 80% of data common to all along track positions at a given time.

298

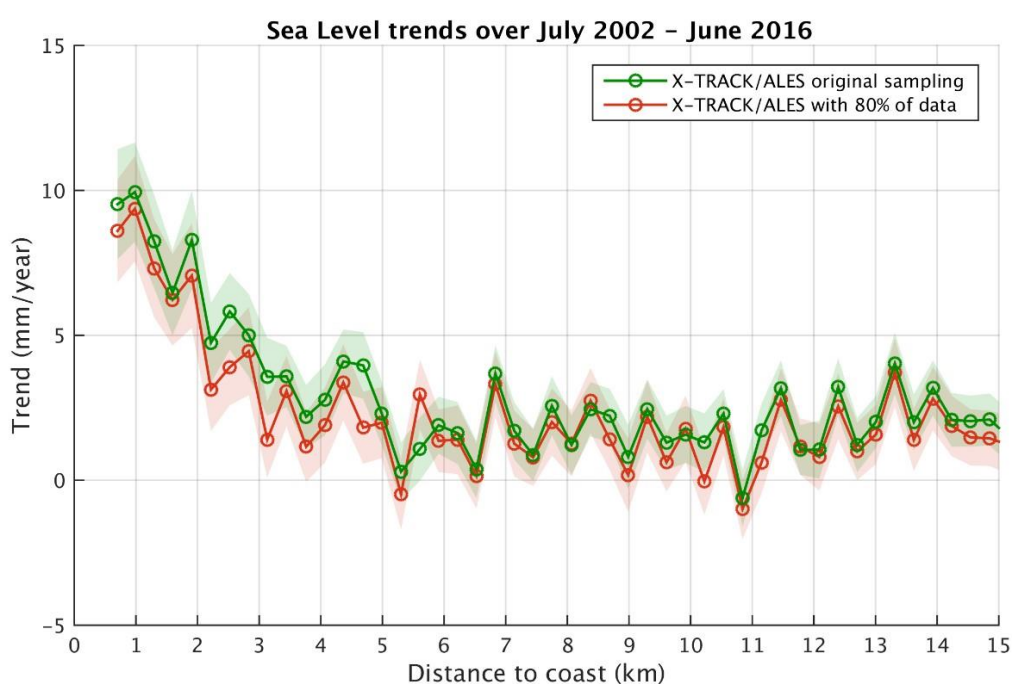
299



300
 301
 302
 303
 304
 305
 306
 307
 308
 309
 310
 311

Fig. 6. Percentage of missing points for the original data set.

The along-track sea level trends were recomputed with the new sampling (80% of the original data kept) (Fig.7). For comparison, in Fig.7 we superimpose the trends computed with the original sampling. Trends compare well in both cases. Even if the trend values are slightly lower in the band 0-5 km, keeping only 80% of the valid data does not change significantly the coastal trend behavior. We conclude that the lower amount of valid near-shore altimetry data does not explain the trend increase observed as the distance to the coast decreases.



312

313

314

315 *Fig. 7. Sea level trends against distance to the coast with the original data set (green curve) and*
316 *new sampling (80% of original data kept; red curve).*

317

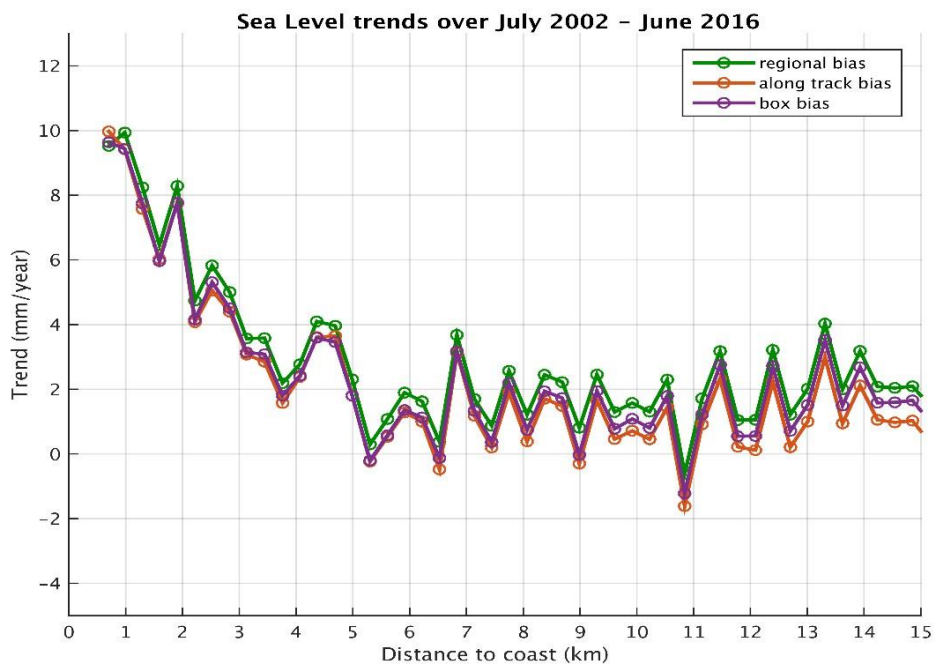
318

319 4.2.3 Effect of intermission bias estimation

320 As discussed in detail in Marti et al. (2019), in the X-TRACK/ALES sea level product, the
321 bias applied to combine the Jason-1 and Jason-2 data in a single sea level time series was
322 estimated at a regional scale. In the case of our study region, it was estimated over the whole
323 Mediterranean Sea. In order to investigate a possible impact of this approach on the sea level
324 trend estimates, we tested other bias calculation methods. We first recomputed the
325 intermission bias along the Jason track 85 (using only measurements of this particular track).
326 In another test, the bias was computed from data included in a 1x1 degree box around the
327 Senetosa site. The sea level trends derived from the corresponding Jason-1 and Jason-2 time
328 series are shown in Fig. 8a for these two cases, superimposed to the regional bias case shown
329 in section 4.1. Here again, we can see that there is almost no difference between the results of
330 the three approaches, indicating that inadequate intermission bias estimate does not explain
331 the coastal trend increase. To complete these tests, we also recomputed SLA trends as a
332 function of distance to coast using as reference a local geoid computed for altimetry mission
333 calibration purposes (P. Bonnefond, personal communication). Fig.8b shows the geoid profile
334 together with the along-track mean sea surface computed with the altimetry data, as a function
335 of latitude. Both references compare well. Thus, as expected, exactly the same trend increase
336 behavior against distance to coast is observed when the reference geoid is used (figure
337 not shown as it is similar to Fig.4). We conclude that the reference has no impact on the
338 computed trends.

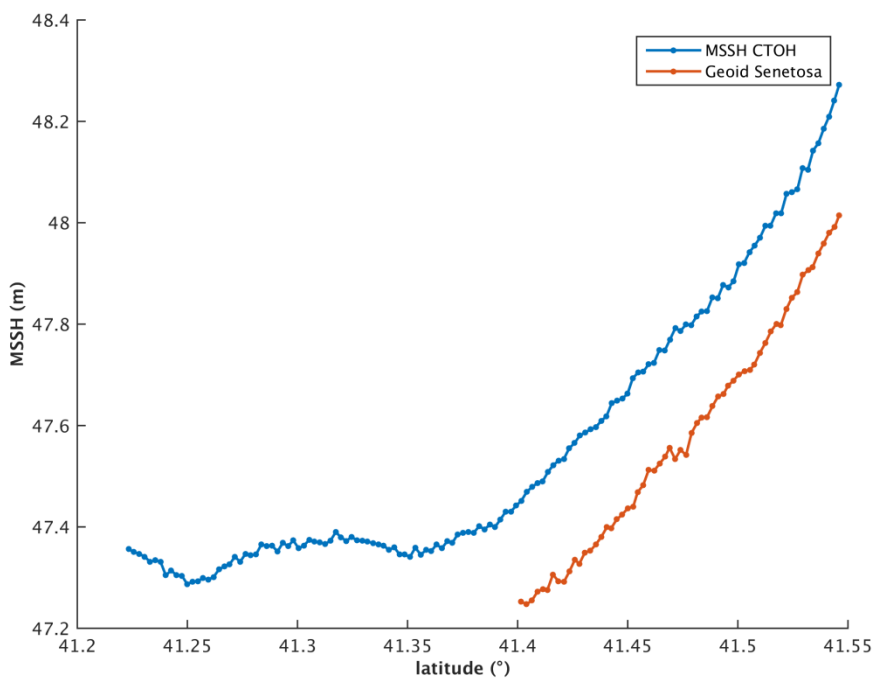
339

340 (a)
341
342



343
344
345
346
347

348 (b)
349
350
351



352
353
354

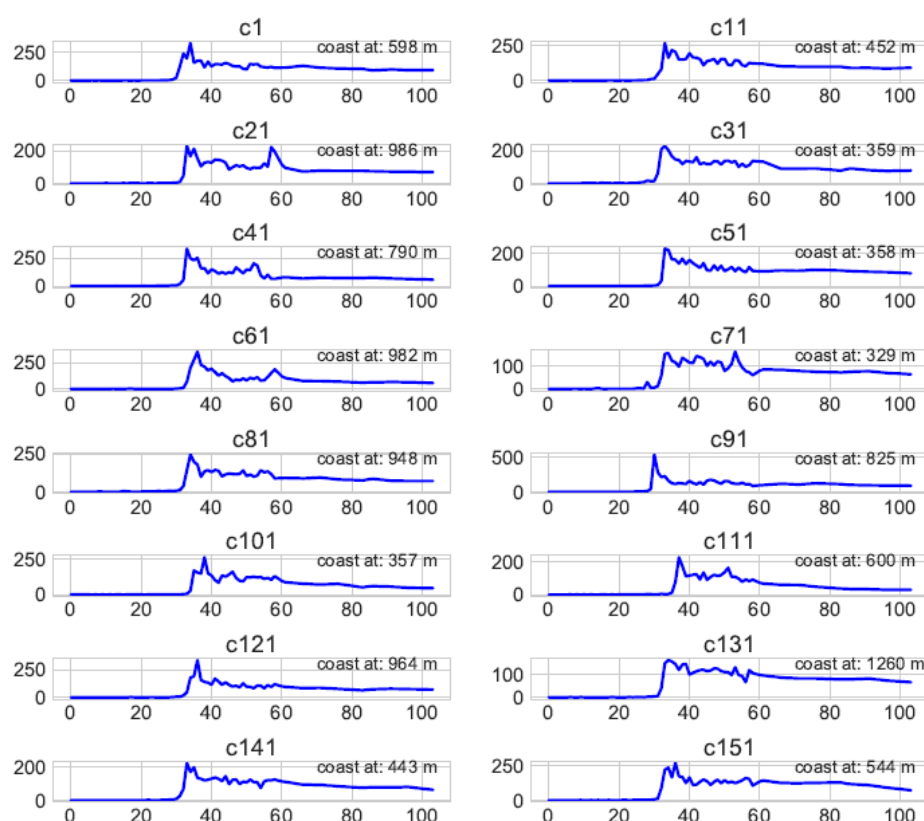
355 *Fig.8. (a) Sea level trends against distance to the coast for three different intermission bias*
356 *estimates. (b) Geoid and altimetry-based along-track mean sea surface profiles against*
357 *latitude.*

358
359

360 4.2.4 Coastal altimetry waveforms and range values near Senetosa

361 In another series of tests, we examined the shape of the radar waveforms at 20 Hz points as a
362 function of distance to coast, considering a few Jason cycles taken at random. An example is
363 shown in Fig. 9 for a point located between the coast and 2 km offshore. Fig.9 shows that at
364 the Senetosa site, the leading edge of the coastal radar echo is generally well defined,
365 suggesting that a robust determination of the range is possible very close to the coast.

366
367



368
369

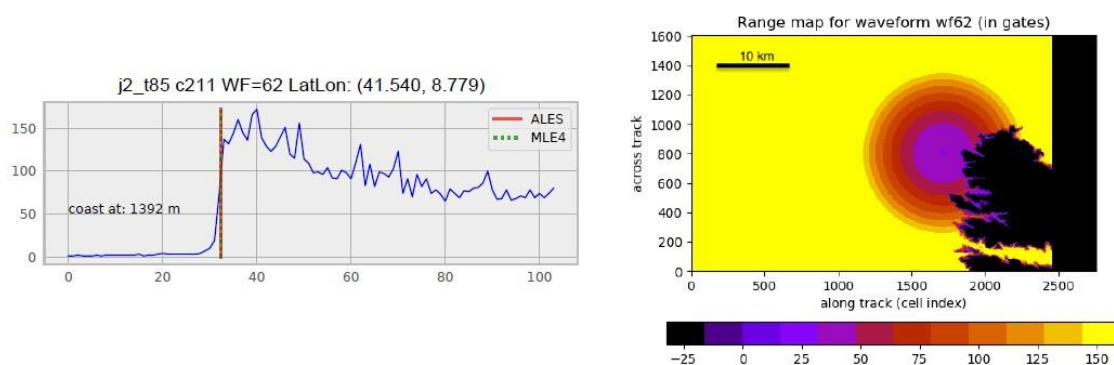
370 *Fig. 9. Observed radar waveforms at points close to the coast for a series of Jason cycles*
371 *(numbers on each plot refer to cycle number).*

373 To investigate this further, we tried to assess the reliability of successive 20-Hz ALES-based
374 range data very close to the coast. The waveform amplitude represents the radar power as a
375

376
 377 function of time. For Jason-2, time is discretized into 104 successive ‘gates’. Knowledge of
 378 the orbit and radar footprint allows by simple geometric analysis to associate a point on
 379 ground (pixel) to a given gate. A numerical simulation has been performed for that purpose
 380 (assuming flat land) in order to produce range maps for the Jason track 85, with the goal of
 381 precisely locating the point on ground corresponding to the measured waveform. This is
 382 illustrated on Fig. 10a and Fig. 10b, showing the geographical configuration and associated
 383 radar waveforms for two range measurements located at 0.53 km and 1.4 km distance from
 384 coast. The range measurement deduced from the waveform corresponds to the center of the
 385 circle representing the radar footprint on the range map.

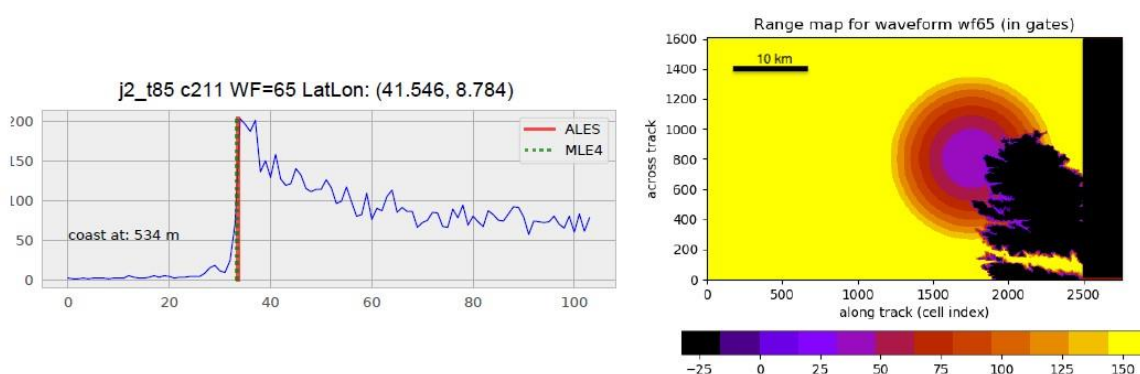
386
 387
 388
 389
 390

(a)



391

(b)



394
 395

396 *Fig. 10. (a) Radar waveform against gate number (left) and configuration of the radar*
 397 *footprint on ground (right) at 1.4 km from coast. (b) Same as (a) at 0.5 km from coast.*

398
 399

400 Although these simulations represent an ideal case of smooth sea state and flat land, Fig.
 401 10a,b shows that even at the closest point to coast (0.5 km), the leading edge of the return

402

403 waveform still corresponds to a reflection of the radar signal on water. This suggests that it is
404 theoretically possible to retrieve valid sea level information up to 0.5 km to the coast. One
405 may argue that because the land at Senetosa has some elevation, the real radar echo is partly
406 contaminated by land reflection at distances larger than the theoretical footprint, even if there
407 is no wave. However, considering that the real waveform has a leading edge, and t h a t
408 the retracker is able to follow it, we conclude that the trends reported on successive 20-Hz
409 points are not spurious. Besides, if the retracker was corrupted by inhomogeneous backscatter
410 properties within the satellite footprint, these should be random (e.g., Passaro et al. 2014).
411 Finally, 20-Hz waveforms being independent samples, if the retracker is wrong and produces
412 spurious trends, the latter also would be random. Thus, we should not see a continuous trend
413 increase over several consecutive points.

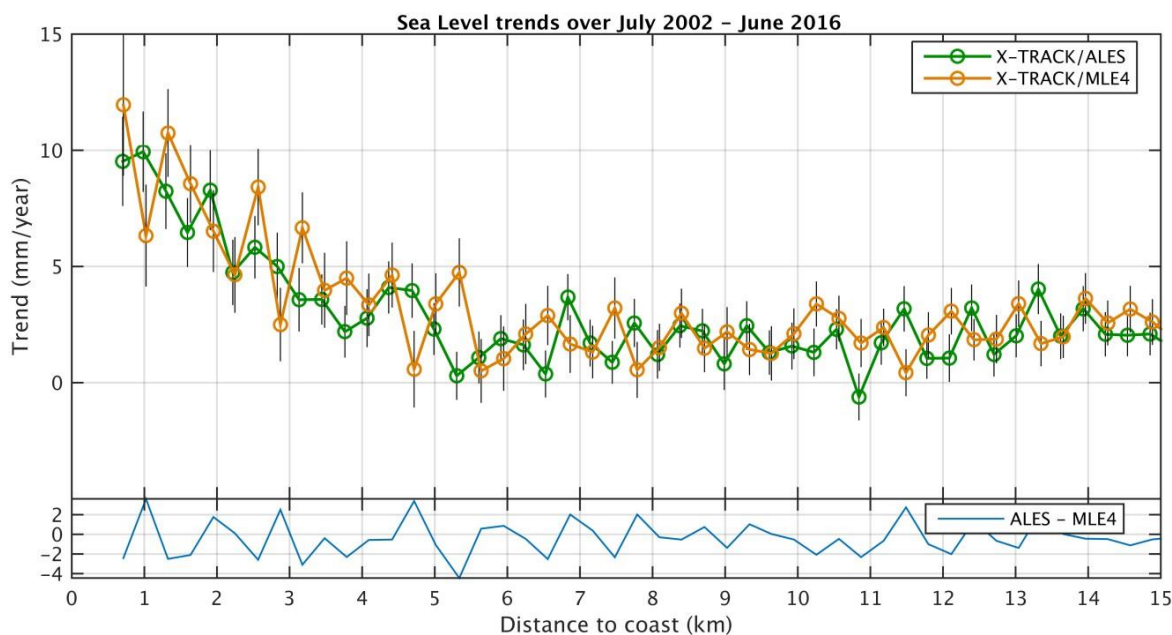
414

415 4.2.6 Comparison between ALES and MLE4 retrackers

416 Finally, we performed the same analysis (computation of sea level trends as a function of
417 distance to the coast) using SLA data computed with the classical MLE4 retracker (used for
418 the standard Geophysical Data Records production,
419 https://www.aviso.altimetry.fr/fileadmin/documents/data/tools/hdbk_tp_gdrm.pdf). MLE4-
420 based trends over the 14-year time span are shown in Fig. 11, on which are superimposed the
421 ALES-based trends, for comparison. We note that MLE4 gives noisier results than ALES,
422 especially at distances less than ~5 km to the coast, but the increase in trends in the last ~4-5
423 km to the coast is still well visible. This clearly means that the trend increase is not an artifact
424 due to the use of the ALES retracker.

425

426



427

428

429

430

431 *Fig. 11. Sea level trends against distance to the coast for MLE4 (orange dots) and ALES*
 432 *(green dots)-based SLA data. Vertical bars correspond to trend errors (1-sigma). The light*
 433 *blue curve at the bottom of the panel represents the difference between ALES-based and MLE4-*
 434 *based trends.*

435

436

437

438 To summarize, from all the tests presented above, we can conclude that the increase in
 439 altimetry sea level trend observed in the last 4-5 km to the coast is not correlated with errors
 440 in the geophysical corrections, is not explained by the loss of valid data, nor the presence of
 441 spurious waveforms or by the intermission bias. Furthermore, the calculated trends are robust
 442 to change in retracker, since instead of using ALES, we also used the standard high-frequency
 443 MLE4 retracker. The corresponding time series still show the same trend behavior (although
 444 with noisier results).

445

446 **5. Comparison with the sea level trend derived from tide gauges records**

447 It is very classical to validate altimetry-based sea level data by comparing with tide gauge
 448 records. The availability of tide gauge records at the Senetosa site is a good opportunity to do
 449 so. Tide gauge data have been provided by the Observatoire de la Côte d'Azur (Géoazur
 450 laboratory) and downloaded from [www.aviso.altimetry/fr/en/data/calval/in-situ/absolute-](http://www.aviso.altimetry.fr/en/data/calval/in-situ/absolute-calibration/download-tide-gauge-data.html)
 451 [calibration/download-tide-gauge-data.html](http://www.aviso.altimetry.fr/en/data/calval/in-situ/absolute-calibration/download-tide-gauge-data.html). The high-frequency tidal signal and the
 452 atmospheric forcing effect have been removed (using the same DAC correction as for the

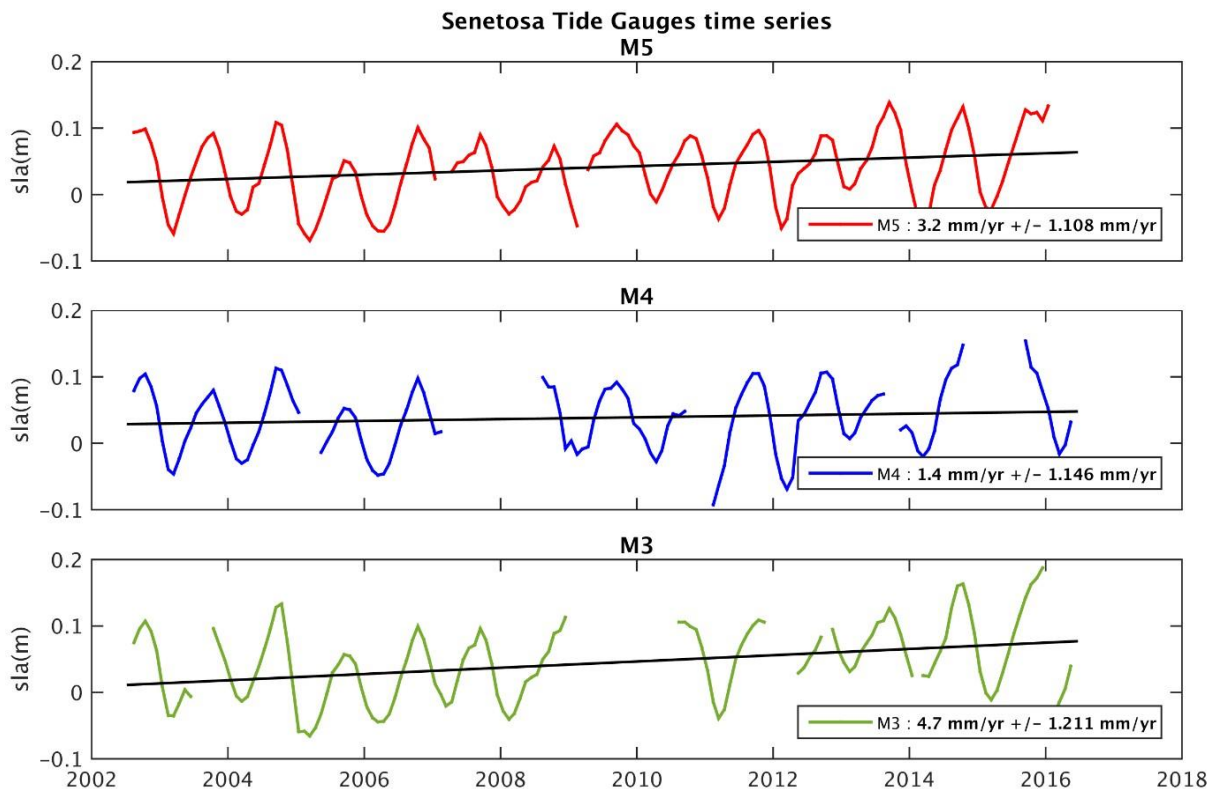
453

454 altimetry data). The time series have been further smoothed on a monthly basis. The
455 corresponding tide gauge time series over 2002-2016, for the M3, M4 and M5 tide gauges, are
456 shown in Fig. 12a and 12b, with and without the seasonal cycles.

457

458
459

(a)

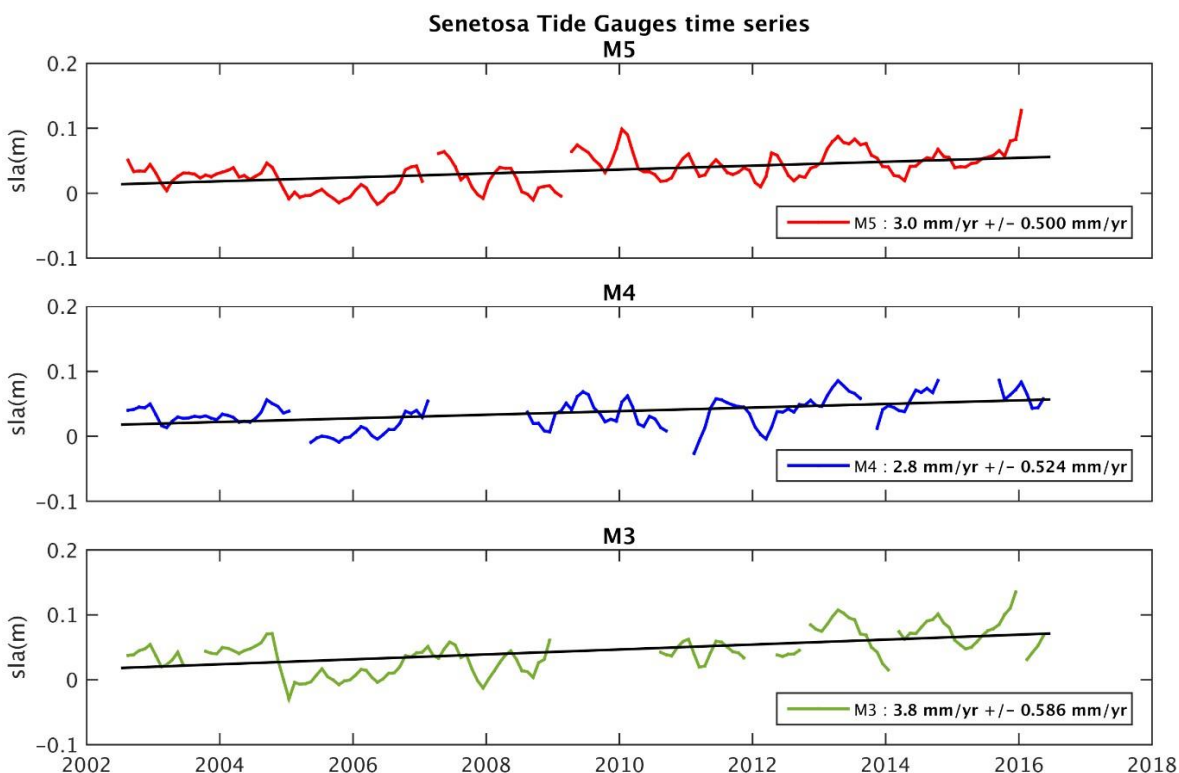


460

461

462

(b)



463

464
465
466
467
468
469
470
471
472
473
474
475
476
477
478

Fig. 12. Sea level time series based on in situ tide gauges measurements at the M3, M4 and M5 sites over 2002-2016. (a) With the seasonal cycle. (b) Without the seasonal cycle.

From these time series, we computed linear trends over the same period as for the altimetry data. These are gathered in Table 2 for the two cases (with and without the seasonal cycle). In Bonnefond et al. (2019), it was shown that when making differences between tide gauges sea level measurements, there is no systematic trend between the tide gauge time series since 2001 (below 0.1 mm/yr), well within the trend uncertainties. The GNSS-based vertical land motion (VLM) at Senetosa (estimated in Bonnefond et al., 2019) is also shown. VLM is small at Senetosa, less than 0.3 mm/yr.

Tide Gauge	Tide gauge trend (mm/yr) (with seasonal cycles)	Tide gauge trend (mm/yr) without seasonal cycles	GNSS VLM (2003-present) (mm/yr)
M3	4.7 +/- 1.2	3.8 +/- 0.6	0.28 +/- 0.05
M4	1.4 +/- 1.1	2.8 +/- 0.5	0.28 +/- 0.05
M5	3.2 +/- 1.1	3.0 +/- 0.5	0.28 +/- 0.05

479

Table 2. Relative sea level trends (mm/yr) recorded by the M3, M4 and M5 tide gauges (estimated with and without the seasonal cycles) as well as the GNSS-based vertical land motion (mm/yr) at the Senetosa site.

483

The M4 time series displays several gaps over the study period. In addition, the record (seasonal cycle not removed, Fig. 12a) shows a large positive anomaly in 2015, not seen by M3 neither M5. M3 has also a large gap in 2009/2010, as well as other gaps 2012 and at the end of the record. A suspect drop is also visible in 2005 on Fig. 12b (seasonal cycle removed). Thus the M5 record seems the most reliable, even if the trends from M3 and M4 are close to M5 (see Table 2). The computed (relative) sea level trend (uncorrected for the VLM) is on the order of 2.8-3.8 mm/yr over the study period (seasonal cycle removed). If the GNSS VLM trend is accounted for, this range becomes 3.1-4.1 mm/yr. This value is significantly less than the altimetry-based sea level trends reported here in the last 4-5 km to the coast. On the other hand, the tide gauge trend agree well with the altimetry-based trends reported at distances greater than > 4 km from coast. While the reported altimetry-based sea level trend increase may disqualify our retracked sea level data in the vicinity of the coast, in

495

496

497 the next section we discuss the possibility that some coastal processes affect sea level in a
498 band of a few km from the coast while being attenuated very close to the shore where the tide
499 gauges (in particular M5) are located. .

500

501 **6. Small scale coastal processes**

502 Compared to deep-ocean sea level, sea level close to the coast can be impacted by various
503 small-scales processes resulting from the morphology of the coastline, the depth of the
504 continental shelf, the presence of a river estuary, etc. (Woodworth et al., 2019). Thus coastal
505 sea level may significantly differ from open ocean sea level over a large range of temporal
506 scales. In terms of trends, the open ocean sea level essentially results from processes affecting
507 the global mean sea level (mean ocean thermal expansion, land ice melt and land water
508 storage changes) (e.g., WCRP, 2018) and the superimposed regional variability (regional
509 changes in ocean thermal expansion, atmospheric loading and fingerprints due to the solid
510 Earth response to changing ice mass loads; Stammer et al., 2013). At the coast, in addition of
511 these two contributions, local variations in other processes may cause additional small-scale
512 sea level changes at interannual to decadal time scales, such as trapped Kelvin waves,
513 upwelling/downwelling effects, eddies, wind-generated waves and swells, shelf currents, water
514 density changes related with river runoff in estuaries (see Woodworth et al., 2019 for a detailed
515 discussion on forcing factors affecting sea level changes at the coast). Note that we do not
516 discuss vertical land motion here since our objective is to understand the observed change
517 in ‘geocentric’ sea level as measured by satellite altimetry.

518 In the case of Senetosa, river runoff and trapped Kelvin waves are not supposed to affect
519 coastal sea level. Could other processes like trends in wind-generated waves and coastal
520 currents explain the slow increase in sea level trend towards the coast? These are discussed
521 below.

522

523 **6.1 Effect of waves on SLA and SSB**

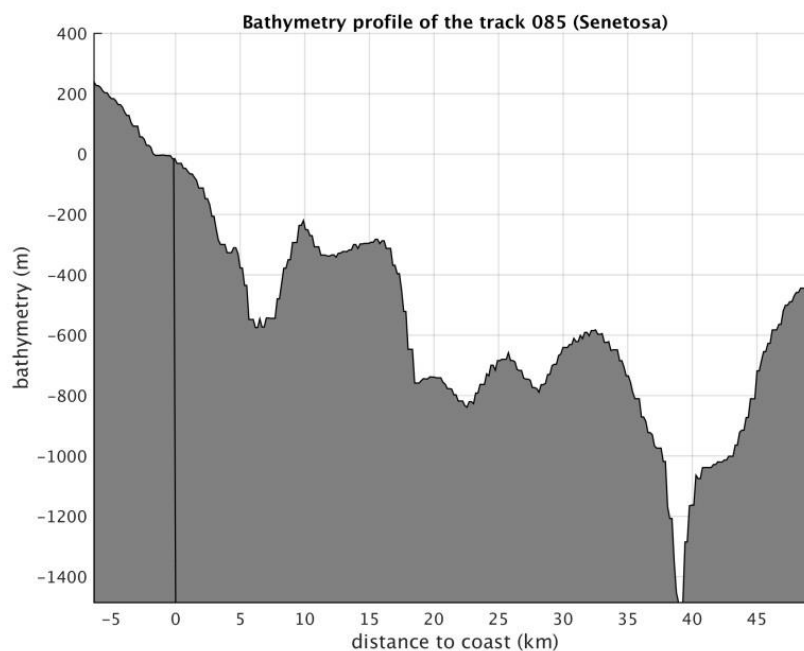
524 We first discuss the effect of waves. The contribution of wind-generated waves to coastal sea
525 level changes has been investigated in a number of recent studies (e.g., Melet et al., 2018,
526 Dodet et al., 2019). As thoroughly discussed in Dodet et al. (2019), wind-generated waves
527 have the capability to significantly change sea level variations at the coast, even at the time
528 scales of interest here. The shoaling and breaking of waves in the shelf shallow waters raises
529 the mean water level in the so-called near-shore and surf zones (last ~1 km to coast), a

530

531 process called wave set-up. Wave set-up is proportional to offshore significant wave height,
 532 and if the latter displays a temporal trend due to a trend in wind forcing, it may cause a sea
 533 level trend in the coastal zone.

534 The relationship between offshore wave height and wave set-up is known empirically only
 535 (Dodet et al., 2019). To first order, wave set-up is related to offshore SWH, wave period and
 536 beach slope. The bathymetric profile along the Jason track 85 (from 45 km offshore to coast)
 537 is shown in Fig. 13. We note an abrupt increase of more than 500 m in the last 5 km to coast,
 538 corresponding to a slope of 0.1.

539



540

541

542 *Fig. 13. Bathymetric profile (meters) along Jason track 85 from 45 km offshore to coast*

543

544

545 If the bathymetric slope near Senetosa is known, it is not the case for other parameters
 546 involved in the relationship between SWH and wave set-up. This is the case in particular for
 547 beach soil characteristics, sediment size, etc. A large variety of formulations have been
 548 proposed for this relationship, based on in situ observations collected at different coastal sites
 549 (e.g., Dodet et al., 2019). However, these are not necessarily applicable to our study case as
 550 some local beach parameters are not known. But it is generally assumed that wave set up does
 551 not exceed 20% of SWH. Thus, as a preliminary approach, we analyzed offshore SWH data
 552 only, in order to highlight their temporal variability over our study time span.

553 For that purpose we considered wave field data from the ERA5 reanalysis
 554 (<https://www.ecmwf.int/en/forecasts/datasets/reanalysis-datasets/era5>;
 555 <https://apps.ecmwf.int/data-catalogues/era5/?class=ea>). The ERA5 reanalysis

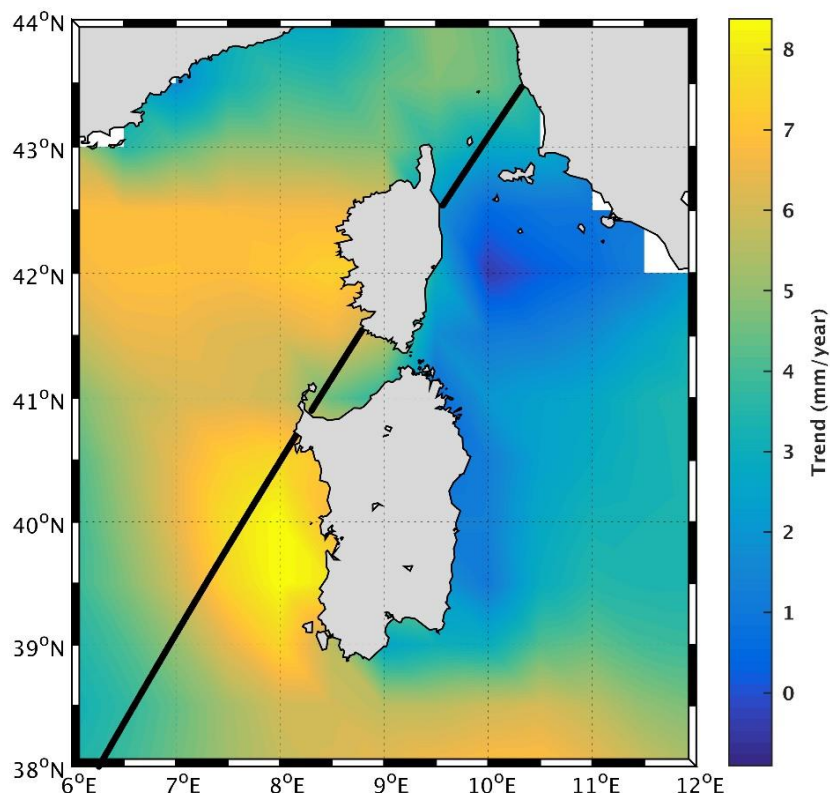
556

557 provides gridded SWH time series at monthly interval, from 1979-present, thus covering our
 558 study period. The grid size resolution is 0.5 degree. Using this data set, we computed 2-D
 559 SWH trends over 2002-2016, shown in Fig. 14. We note high positive wave height trends
 560 west of Corsica and Sardinia over this period. Along the Jason track 85, in the vicinity of
 561 Senetosia, the trend is on the order of 5 mm/yr. Note that we also computed the wind trend using
 562 the same ERA5 reanalysis gridded data over the same period (2002-2016). The map (not shown)
 563 displays positive trends in wind south of Corsica, although with smaller amplitude than along
 564 the western coast of Sardinia, like the wave height map shown in Fig.14.

565 From the above discussion, we deduce that wave set up would not contribute by more than 1
 566 mm/yr to the coastal sea level trend. Noting in addition that wave set up would affect sea level
 567 in the close vicinity of the coast only (i.e., not over 4-5 km distance, X. Bertin, and J. Wolf,
 568 personal communications), it is very unlikely that wave set up explains the reported coastal
 569 sea level trend.

570

571



572

573

574 *Fig. 14. Wave height trends (in mm/yr) over 2002-2016 in the western Mediterranean Sea*
 575 *(data from ERA5 reanalysis)*

576

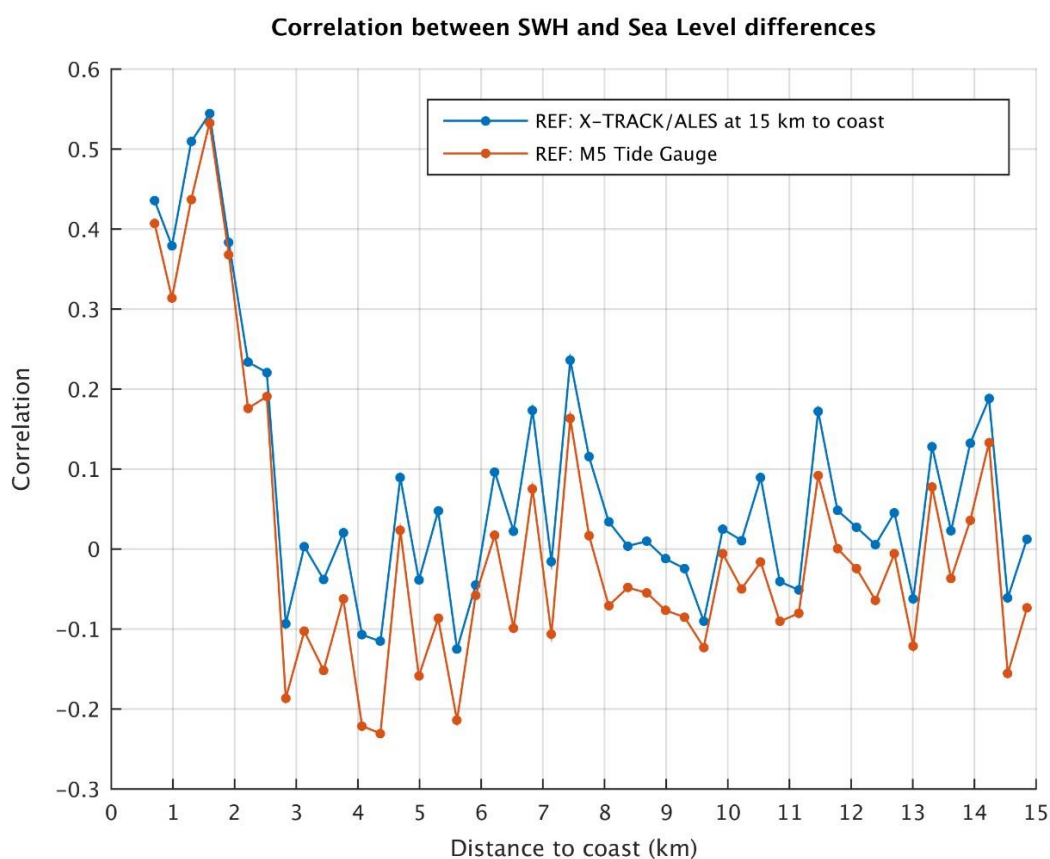
577 We further investigated the effect of waves on the ssb correction, hence on SLAs. For that
 578 purpose, we computed the correlation between wave height time series and difference in sea

579 level between each 20 Hz altimetry point and a reference altimetry point located in the

580 open ocean (chosen here at 15 km from the coast). We consider differences in sea level
 581 anomalies in order to remove the common ocean signal affecting sea level close to the
 582 coast and offshore, e.g., the global mean sea level rise and its superimposed regional
 583 variability. By computing the sea level differences between 15 km offshore and
 584 coast, the latter large-scale sea level components are removed, leaving only
 585 small-scale signals occurring very close to the coast. Data from the ERA5 grid
 586 closest to Senetosa were used (the center of the considered grid point is located 41.5°N, 8.5°E, at
 587 24 km from the first valid point on the Jason track and 25 km from Senetosa). The correlation
 588 values are shown in Fig. 15 against distance to the coast. From a distance of ~3 km from the
 589 coast towards the deep sea, the correlation between wave height and sea level difference is
 590 insignificant while it clearly increases from ~3 km to the coast. This suggests that there is a
 591 link between the variations in waves and SLA variations in the 0-3 km domain close to land.

592 We performed the same analysis but now using the M5 tide gauge record as reference (the M3
 593 tide gauge record having too many data gaps). This is also shown in Fig. 15. Surprisingly, we
 594 find exactly the same behavior of the correlation coefficient, i.e., no correlation offshore
 595 (points located at distance > 3 km from coast) and an increase in correlation in the last 3 km
 596 to the coast. This suggests that waves may affect SLA only in the domain 0-3 km from
 597 coast but that at the tide gauge site, waves have no influence. Obviously, this could be via
 598 the ssb correction applied to SLA data.

599
 600



601

602

603 *Fig. 15. Correlation between the wave height (SWH) time series (from ERA5 grid mesh close*
604 *to Senetosa) and altimetry-based sea level difference time series between every 20 Hz point*
605 *and a reference point. The blue curve corresponds to a reference time series for a point*
606 *located at 15 km from the coast. In the case of the red curve, the reference time series is the*
607 *M5 tide gauge record.*

608

609 It has been demonstrated that applying the ssb correction to altimetry data, in particular to high-
610 frequency data as in this study, reduces the correlation between SWH and range (and,
611 consequently, SLA) (Passaro et al., 2018). The ssb correction is mainly a function of SWH: it
612 removes from the range estimation an effect that is directly proportional to the wave height.
613 This means that if this ssb correction is not applied, it has to be expected that the SLA record
614 will be correlated with the SWH record. To illustrate this somewhat differently, Fig. 16a shows
615 wave height time series superimposed to altimetry-based difference in SLA time series
616 (reference point at 15 km, as in Fig. 15) for a few points located in the 0-3 km domain close
617 to the coast and an additional point located farther from the coast. Here again, data from
618 the ERA5 grid closest to Senetosa have been considered for the calculation. The correlation
619 between SWH and difference SLA time series is indicated on each plot. We clearly see that
620 it is significant only for points close to the coast. Distant offshore points do not show such
621 a correlation. Although the correlation is dominated by the seasonal signal, Fig. 16 shows
622 the two time series are also correlated at interannual time scales.

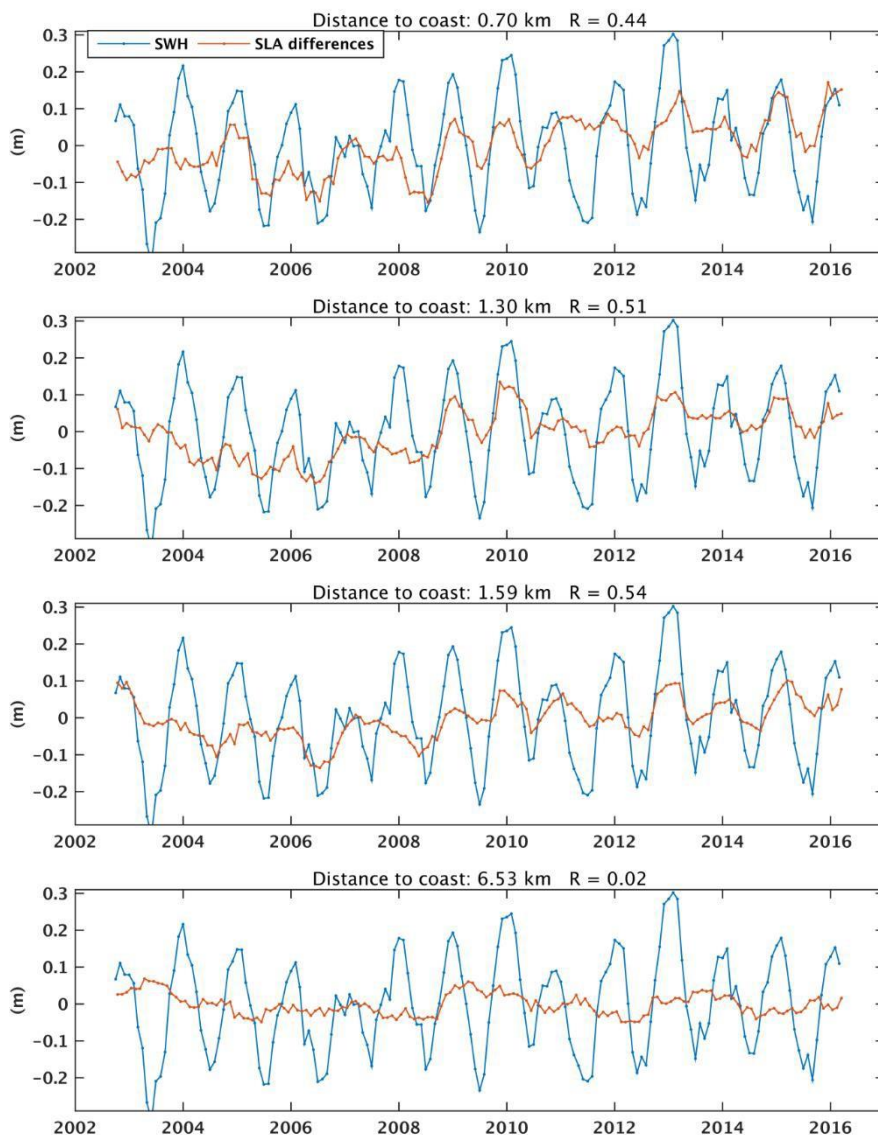
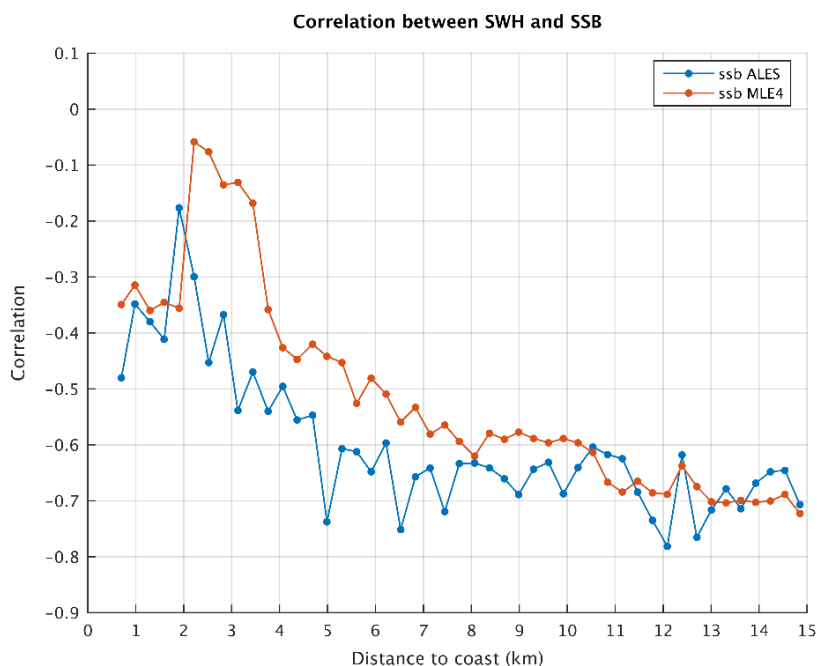


Fig. 16: Time series of ERA5-based wave height time series (blue curve) and of altimetry-based SLA differences (orange curve) between 20 Hz points at different distances from coast (indicated on each plot) and a reference point (located at 15 km).

We argue that when the range close to the coast is not being properly corrected for the ssb, this results in a lesser correlation between ssb and SWH. To verify this, we repeated this correlation analysis but now using the ssb correction (from both the ALES and MLE4 retrackings) instead of the SLA differences. As expected, ssb is correlated with SWH away from the coast (of -0.75 and -0.56 at 6.5 km from the coast for MLE4 and ALES respectively), but the correlation decreases in the last few km to the coast (amounting -0.35 and -0.48 at 0.7 km from the coast for MLE4 and ALES respectively). This suggests that the relationship used to express the link between ssb and SWH is less adapted in the coastal domain than in the open sea, either because of change of wave properties (which makes the ssb model invalid)

678 or because of a wrong estimation of SWH very close to the coast. This is also illustrated in Fig.
679 17 that shows the correlation between ssb and SWH against to distance to the coast (for both
680 ALES ssb and MLE4 ssb). Between 1 km

681
 682 and 4 km, the correlation between SWH and ssb decreases. It is worth noting however that
 683 the correlation remains higher for ALES ssb than for MLE4 ssb.
 684



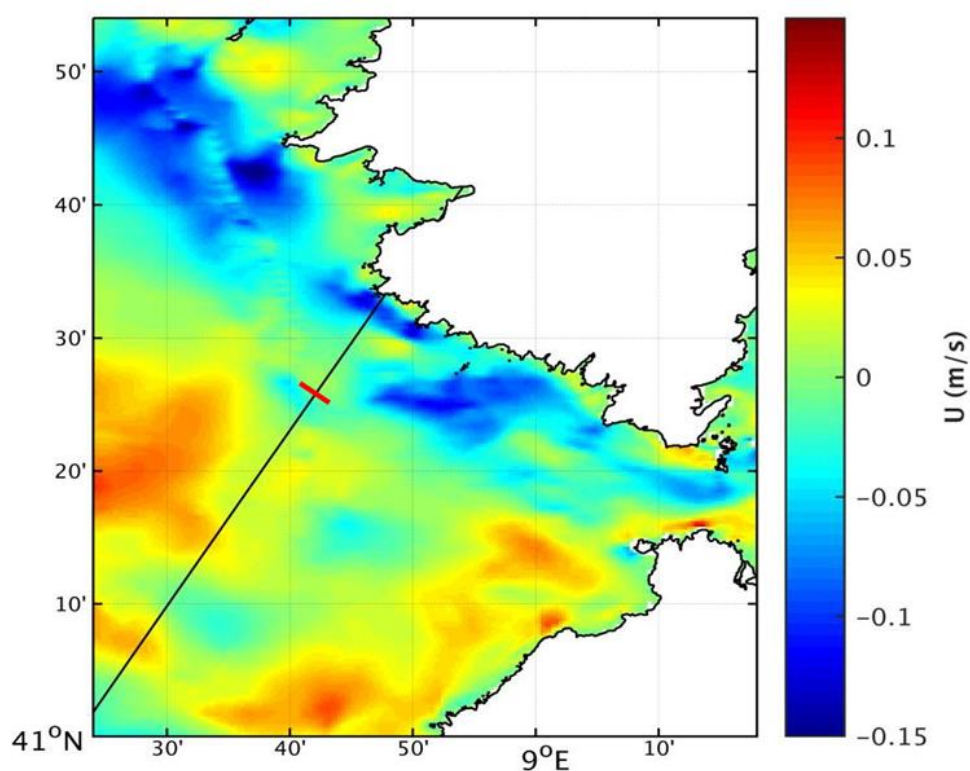
685
 686
 687 Fig. 17. Correlation between significant wave height (SWH) time series and ssb time series
 688 between every 20 Hz point and a reference point.

689
 690 We conclude from these tests, that the correlation between SLA and wave height at 20 Hz
 691 points close to the coast is very likely due to imperfect ssb correction. Thus we can now
 692 exclude any direct effect of waves (e.g., trend in wave set-up) as a candidate to explain the
 693 SLA trend increase close to the coast. Are the reported SLA trends in the last few km to the
 694 coast due to inadequate formulation of the relationship between SWH and ssb as the satellite
 695 approaches the coast remains so far an open question. While we cannot exclude that the ssb
 696 correction is imperfect close to the coast, it seems unlikely that it would produce such large
 697 trends as those observed in the SLAs.

698
 699 **6.2. Effect of coastal currents and comparison with an ocean model**
 700 In this section we briefly address the effect of coastal currents on the SLAs. There are only
 701 few published studies on the circulation in the Senetosa region (e.g., Bruschi et al., 1981,
 702 Manzena et al., 1985, Cucco et al., 2012, Gerigny et al., 2015, Sciascia et al., 2019). These
 703 indicate that the dominant characteristics of the circulation in the Corsica channel (Bonifacio
 704 Straits) is a flow predominantly directed northward from the Tyrrhenian Sea to the Ligurian

705

706 Sea and that the water motion is mainly wind-driven. The study by Gerigny et al. (2015)
707 based on in situ measurements collected during a cruise in 2012 and use of a high-resolution
708 regional hydrodynamic model (MARS3D) shows that the circulation is mostly wind-driven,
709 forced by westerly winds half of the year and strong easterly winds in winter, generating strong
710 local currents and mesoscale structures in the western part of the channel. We have
711 downloaded the currents data generated by the MARS3D model, a coastal hydrodynamical
712 model developed by IFREMER (Institut Français de Recherche pour l'Exploitation de la
713 Mer; Lazure and Dumas 2008). There is a high-resolution (400 m) version available for the
714 Corsica region, for the years 2014 to present
715 (<http://www.ifremer.fr/docmars/html/doc.basic.intro.html>). The model does not assimilate
716 altimetry data nor any other type of data. Because this dataset has only 2.5 years of overlap with
717 our study period, we cannot compute trends. However, to gain some insight on the circulation
718 configuration, we examined the currents pattern over the year 2014. In agreement with the
719 literature, we observed a strong zonal current during the winter months close to Senetosa. An
720 example of the zonal component of the barotropic current south of Corsica is shown in Fig.18
721 for January 2014. We note a clear westward current along the Senetosa coast starting at ~4 km
722 from the coast. It is also worth noting that it does not extend to the shoreline, thus may not
723 influence tide gauge measurements.
724



725

726

727 *Fig.18. Barotropic current (zonal component) for January 2014 based on the MARS3D*
 728 *hydrographic model. Blue color means westward current. The Jason track (black line) crosses*
 729 *this current at 4 km from the coast. The red bar crossing the Jason track indicates the 15 km*
 730 *distance from the coast.*

731

732 We interpolated these current data (for January 2014) along the Jason track. This is shown in
 733 Fig.19 against distance to the coast. The current intensity is close to zero at distances >5km from
 734 the coast. In the last 5 km to the coast, there is a steep intensity increase, exactly over the same
 735 distance range as the SLA trend increase. Since the model resolution is ~400m, i.e., about the
 736 same resolution as the 20 Hz along-track SLAs, we find this result highly promising.

737

738

739

740

741

742

743

744

745

746

747

748

749

750

751

752

753

754

755

756

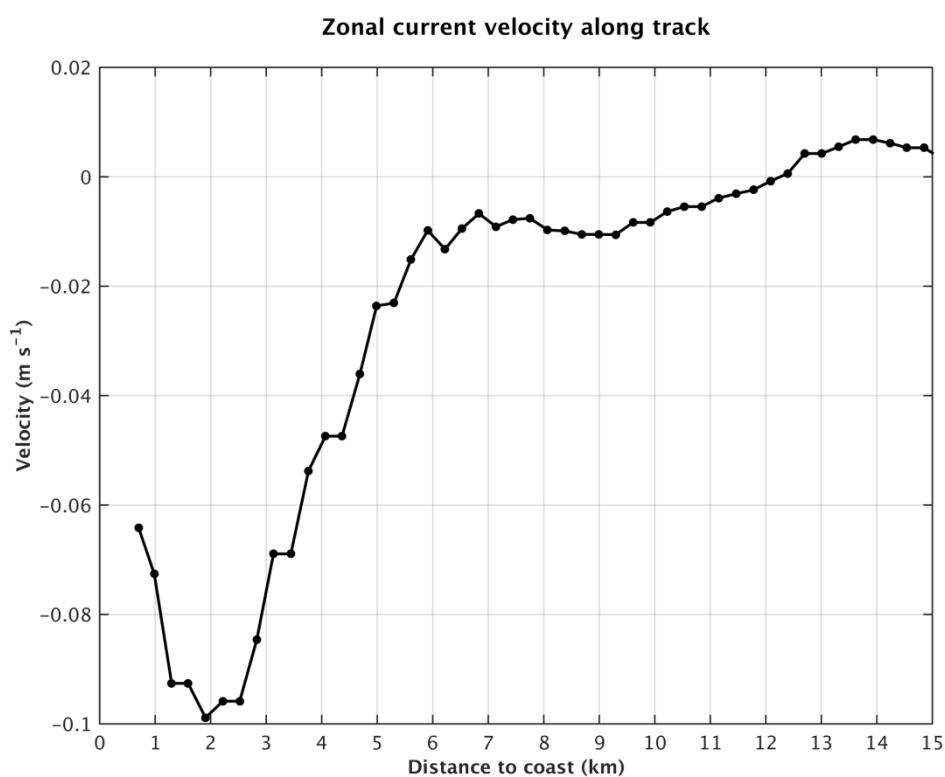
757

758

759

760

761



762 *Fig.19. Barotropic current (zonal component) for January 2014 based on the MARS3D*
 763 *hydrographic model interpolated along the Jason track, against distance to the coast.*
 764 *Negative values mean westward current.*

765

766 Of course, we cannot extrapolate backward in time nor offer any solid conclusion so far. But we
 767 cannot exclude that the observed sea level trend increase is linked to an increase in intensity of
 768 this winter current during our study period. This obviously will need much deeper investigation,
 769 at least over the time span of availability of the model data.

770

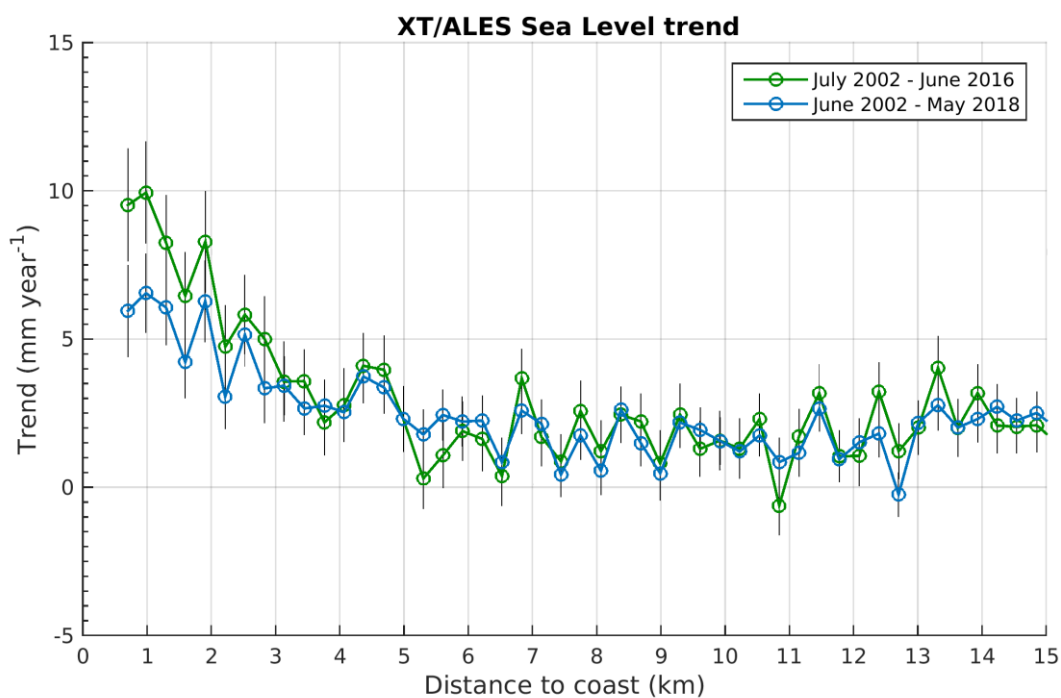
771 **7. Conclusion**

772 In this study, we have investigated the differences between coastal and deep ocean sea level
773 changes at the Senetosa site, using new ALES-based retracked sea level data from the Jason-1
774 and Jason-2 missions. We indeed observe a slow increase in sea level trend at short ($< \sim 4\text{-}5$
775 km) distance from the coast compared to offshore. A series of test shows that this behavior
776 does not result from artifacts due to spurious trends in the geophysical corrections applied to
777 the altimetry data, decreasing percentage of valid data, or errors in the intermission bias nor
778 errors in range estimates due to distorted radar waveforms.

779 While the paper was in review, an update of the results presented above has been recently
780 performed extending the SLA time series with Jason-3 data up to June 2018 (coastal trends based
781 on Jason-1, 2 and 3 over 2002-2018 at several hundreds of coastal sites located in six different
782 regions worldwide are presented elsewhere; The Climate Change Initiative Coastal Sea Level
783 Team, 2020). Although the coastal trends within the 2-3 km to the coast are slightly lower than
784 those reported above, exactly the same behavior is found, as shown in Fig.20 that compares
785 coastal trends over 2002-2016 and 2002-2018. Thus, the trend increase close to the coast
786 observed at Senetosa is not due to the limited length of the time series, although its amplitude
787 decreases as the record length increases. Similarly, the geophysical correction trends present the
788 same behavior over both time spans. It is worth mentioning that in the extended study (2002-
789 2018), among the 429 studied coastal sites, coastal trends do not in general differ from open
790 ocean trends (within ± 1 mm/yr), except at a few sites (The Climate Change Initiative Coastal
791 Sea Level Team, 2020), Senetosa is one of them. This is why we made a focus on that particular
792 site.

793

794



795 *Fig.20. Altimetry-based sea level trends at Senetosa, over two periods: (1) July 2002-June*
 796 *2016, green curve and (2) June 2002-May 2018, blue curve. Black vertical bars*
 797 *correspond to trend uncertainties.*

798

799 Among the physical mechanisms able to explain the coastal trend increase in the study region,
 800 we have first explored waves, then currents. We investigated the wave effect on sea level
 801 along the Jason track and found that wave set up has a too small magnitude and is localized
 802 too close to the shore to explain the observed continuous SLA trend increase in the last 4-5
 803 km to the coast. On the other hand, the correlation reported between altimetry-based SLAs
 804 and SWH very likely results from the imperfect ssb correction applied to the data.
 805 Nevertheless, if less accurate in the coast vicinity, the ssb trend seems unable to explain the
 806 reported SLA trend increase. We next investigated the effect of coastal currents. Using the
 807 MARS3D high resolution model developed by IFREMER for coastal studies, we noted the
 808 presence of a winter current along the Senetosa coastline. Projection of this current along the
 809 Jason track (for January 2014) shows a step increase in intensity over exactly the same
 810 distance to the coast as the SLA trend increase. This may be an indication of a current-related
 811 origin. More studies are definitely needed to confirm the results presented here. However, if
 812 further investigations confirm the effect of currents, it will be a demonstration that small-
 813 scale processes acting in the vicinity of the coast may have the capability to make coastal sea
 814 level changes drastically different from what we measure offshore with classical altimetry.

815

816

817

818 Acknowledgements

819
820 This study is a contribution to the ESA Climate Change Initiative (CCI+) Sea Level project.
821 Yvan Gouzenes is supported by an engineer grant in the context of this project (ESA SL_cci+
822 contract number 4000126561/19/I-NB). We thank a number of colleagues for very fruitful
823 discussions on the effect of waves on tide gauges and coastal sea level, in particular (by
824 alphabetic order) Angel Amores, Xavier Bertin, Svetlana Jevrejeva, Goneri Le Cozannet,
825 Marta Marcos, Judy Wolf and Phil Woodworth. We also thank two anonymous reviewers and
826 the Editor for their comments and suggestions to improve the manuscript.

827

828 Data Availability

829 The coastal sea level data analyzed in this study are available from the Nature Scientific Data
830 article (The Climate change Initiative Coastal Sea Level Team, 2020, A database of coastal sea
831 level anomalies and associated trends from Jason satellite altimetry from 2002 to 2018). The
832 altimetry-based sea level data can be downloaded from the SEANOE repository with the DOI:
833 <https://doi.org/10.17882/74354>.

834 The gridded sea level data from the Copernicus Climate Change Service are available at
835 <https://climate.copernicus.eu/sea-level>.

836 The Senetosa tide gauge data can be downloaded at [www.aviso.altimetry.fr/en/data/calval/in-](http://www.aviso.altimetry.fr/en/data/calval/in-situ/absolute-calibration/download-tide-gauge-data.html)
837 [situ/absolute-](http://www.aviso.altimetry.fr/en/data/calval/in-situ/absolute-calibration/download-tide-gauge-data.html) calibration/download-tide-gauge-data.html

838 The ERA wave field data from the ERA5 reanalysis are available from the following
839 web site: <https://www.ecmwf.int/en/forecasts/datasets/reanalysis-datasets/era5> (see also
840 <https://apps.ecmwf.int/data-catalogues/era5/?class=ea>).

841 [The MARS3D model can be downloaded from the web site:](http://www.ifremer.fr/docmars/html/doc.basic.intro.html)
842 <http://www.ifremer.fr/docmars/html/doc.basic.intro.html>).

843

844 Author contributions

845 All authors contributed in different parts of the data production and analysis, as well as in
846 writing the manuscript. J.F.L. and A.C. are project manager and science leader of the CCI+
847 Coastal Sea Level project, respectively.

848

849 Competing interest

850 The authors declare no competing financial interest.

851
852
853
854
855
856
857
858
859
860
861
862
863
864
865
866
867
868
869
870
871
872
873
874
875
876
877
878
879
880
881
882
883
884
885
886
887
888
889
890
891
892
893
894
895
896
897
898
899
900
901
902
903
904

References

Ablain M., Legeais J.F., Prandi P., et al., 2017. Altimetry-based sea level, global and regional scales, *Surveys in Geophysics*, 38, 7-31, <https://doi.org/10.1007/s10712-016-9389-8>.

Almar, R., E. Kestenare, J. Reyns, J. et al., 2015. Response of the Bight of Benin (Gulf of Guinea, West Africa) coastline to anthropogenic and natural forcing, Part1: Wave climate variability and impacts on the longshore sediment transport, *Continental Shelf Research*, 110, 48-59, <https://doi.org/10.1016/j.csr.2015.09.020>.

Birol F. and C. Delebecque, 2014. Using high sampling rate (10/20 Hz) altimeter data for the observation of coastal surface currents: A case study over the northwestern Mediterranean Sea, *J. Mar. Syst.*, <https://doi.org/10.1016/j.jmarsys.2013.07.009>.

Birol F., N.X Fuller, F. Lyard, et al., 2017. Coastal applications from nadir altimetry: example of the X-TRACK regional products. *Advances in Space Research*, 59, 936-953, <https://doi.org/10.1016/j.asr.2016.11.005>.

Bruschi A., Buffoni G., Elliott A.J., Manzella G., 1981. A numerical investigation of the wind-driven circulation in the Archipelago of La Maddalena, *Oceanol. Acta*, 4, 3, 289-295.

Bonnefond, P., Exertier, P., Laurain, O., Ménard, Y., Orsoni, A., Jan, G., Jeansou, E., 2003a, Absolute calibration of Jason-1 and TOPEX/Poseidon altimeters in Corsica, in: Special Issue on Jason-1 Calibration/ Validation, Part 1. *Mar. Geod.* 26(3-4), pp. 261-284, <https://doi.org/10.1080/714044521>.

Bonnefond, P., Exertier, P., Laurain, O., Ménard, Y., Orsoni, A., Jeansou, E., Haines, B.J., Kubitschek, D.G., Born, G.H. Leveling sea surface using a GPS catamaran, 2003b, in: Special Issue on Jason-1 Calibration/ Validation, Part 1. *Mar. Geod.* 26(3-4), 319-334, <https://doi.org/10.1080/714044524>.

Bonnefond, P., Exertier, P., Laurain, O., Jan, G., 2010, Absolute calibration of Jason-1 and Jason-2 altimeters in Corsica during the formation flight phase, in: Special Issue on Jason-2 Calibration/Validation, Part 1. *Mar. Geod.* 33(S1), 80-90, <https://doi.org/10.1080/01490419.2010>.

Bonnefond, P., B. Haines and C. Watson. In Situ Calibration and Validation: A Link from Coastal to Open-ocean altimetry, 2011, in Coastal Altimetry, chapter 11, pp 259-296, edited by S. Vignudelli, A. Kostianoy, P. Cipollini, J. Benveniste, Springer, ISBN: 978-3-642-12795-3. https://doi.org/10.1007/978-3-642-12796-0_11

Bonnefond, P., Exertier, P., Laurain, O., Guinle, ., F m nias, ., 201 , Corsica: A 20-Yr Multi-Mission Absolute Altimeter Calibration Site, *Advances in Space Research*, Special Issue « 25 Years of Progress in Radar Altimetry », <https://doi.org/10.1016/j.asr.2019.09.049>.

Carrere, L. and Lyard, F. 2003. Modeling the barotropic response of the global ocean to atmospheric wind and pressure forcing- comparisons with observations. *J. Geophys. Res.* 30 (6), 1275. <http://dx.doi.org/10.1029/2002GL016473>.

Carrere L., Lyard, F., Cancet, M., Guillot, A., Roblou, L., 2012. FES2012: A new global tidal model taking taking advantage of nearly 20 years of altimetry, Proceedings of meeting "20 Years of Altimetry", Venice 2012.

- 905 Cartwright, D. E. and R. J. Taylor, 1971. New computations of the tide-generating potential,
906 *Geophys. J. R. Astron. Soc.*, 23, 45-74.
907
- 908 Cartwright, D. E. and Edden, A. C., 1973. Corrected Tables of Tidal Harmonics. *Geophysical Journal*
909 *of the Royal Astronomical Society*, 33: 253-264. doi:10.1111/j.1365-246X.1973.tb03420.x.
910
- 911 Church, J. A. et al., 2013: Sea Level Change. In: Climate Change 2013: The Physical Science
912 Basis. Contribution of Working Group I to the Fifth Assessment Report of the
913 Intergovernmental Panel on Climate Change [Stocker, T. F., D. Qin, G. K. Plattner, M.
914 Tignor, S. K. Allen, J. Boschung, A. Nauels, Y. Xia, V. Bex and P. M. Midgley (eds.)].

- 915 Cambridge University Press, Cambridge, United Kingdom and New York, NY, USA, 1137-
916 1216.
- 917 Cipollini P., J. Benveniste, F. Birol, et al., 2018. Satellite altimetry in coastal regions. In
918 'Satellite altimetry over the oceans and land surfaces', Stammer & Cazenave Edts, CRC
919 Press, Taylor and Francis Group, Boca Raton, London, New York, pp 343-373,
920 <https://doi.org/10.1201/9781315151779-11>
921
- 922 Climate Change Initiative Coastal Sea level Team (The), 2020, A database of coastal sea level
923 anomalies and associated trends from satellite altimetry from 2002 to 2018, in revision, *Nature*
924 *Scientific Data*.
925
- 926 Cucco A et al., 2012, A high-resolution real-time forecasting system for predicting the fate of
927 oil spills in the Strait of Bonifacio (western Mediterranean Sea), *Marine Pollution Bulletin*,
928 64, 1186-1200, doi:10.1016/j.marpolbul.2012.03.019.
929
- 930 Dieng, H., A. Cazenave, B. Meyssignac and M. Ablain, 2017: New estimate of the current
931 rate of sea level rise from a sea level budget approach. *Geophysical Research Letters*, 44 (8),
932 3744-3751, <https://doi.org/10.1002/2017GL073308>.
933
- 934 Dodet G., Melet A., Ardhuin F., Bertin X ;, Idier D. and Almar R., 2019. The contribution of
935 wind-generated waves to coastal sea level changes, *Surveys in Geophysics*, 40, 1563-1601,
936 <https://doi.org/10.1007/s10712-019-09557-5>.
937
- 938 Durand F., Piecuch C., Cirano M. et al., 2019. Impact of continental freshwater runoff on
939 coastal sea level, *Surveys in Geophysics*, 40:1437–1466, [https://doi.org/10.1007/s10712-019-](https://doi.org/10.1007/s10712-019-09536-w)
940 09536-w.
941
- 942 Fernandes, M.J., Lazaro, C., Ablain, M., Pires, N., 2015. Improved wet path delays for all ESA
943 and reference altimetric missions. *Remote Sens. Environ.* 169, 50–74,
944 <http://dx.doi.org/10.1016/j.rse.2015.07.023>.
- 945 Gerigny O., Coudray S., Lapucci C. , Tomasino C., Bisgambiglia P.A., Galgani F., 2015,
946 Small-scale variability of the current in the Strait of Bonifacio, *Ocean Dynamics*, 65, 8, 1165-
947 1182, <http://dx.doi.org/10.1007/s10236-015-0863-5>.
948
- 949 Jebri, F., Birol, F., Zakardjian, B., Bouffard, J., Sammari, C., 2016. Exploiting coastal altimetry
950 to improve the surface circulation scheme over the Central Mediterranean Sea: circulation In
951 The Central Mediterranean. *J. Geophys. Res. Oceans* 121 (7), 4888–4909. [http://](http://dx.doi.org/10.1002/2016JC011961)
952 dx.doi.org/10.1002/2016JC011961.
953
- 954 Lazure P and Dumas F, 2008, An external–internal mode coupling for a 3D hydrodynamical
955 model for applications at regional scale (MARS), *Advances in Water Resources*, 31:233-250,
956 doi:10.1016/j.advwatres.2007.06.010.
957
- 958 Legeais J.F., Ablain M., Zawadzki L. et al., 2018. An improved and homogeneous altimeter
959 sea level record from the ESA Climate Change Initiative, *Earth Syst. Sci. Data*, 10, 281-301,
960 <https://doi.org/10.5194/essd-10-281-2018>.
961
- 962 Léger F., F. Birol, F. Niño, M. Passaro, F. Marti and A. Cazenave, 2019, "X-Track/Ales
963 Regional Altimeter Product for Coastal Application: Toward a New Multi-Mission Altimetry
964 Product at High Resolution," IGARSS 2019 - 2019 IEEE International Geoscience and Remote
965 Sensing Symposium, Yokohama, Japan, 8271-8274,
966 <https://doi.org/10.1109/IGARSS.2019.8900422>.

- 967
968 Manzella G.M.R., 1985, Fluxes across the Corsica Channel and coastal circulation in the East
969 Ligurian Sea, North-Western Mediterranean, *Oceanol. Acta*, 8, 1, 29-35.
970
971 Marti F., Cazenave A., Birol F., Passaro, M. Leger F., Nino F., Almar R., Benveniste J. and
972 Legeais J.F., 2019, Altimetry-based sea level trends along the coasts of western Africa, *Adv.*
973 *in Space Res.*, published online 24 May2019, <https://doi.org/10.1016/j.asr.2019.05.033>.

- 974
- 975 Melet, A., Almar, R. and Meyssignac, B., 2016. What dominates sea level at the coast: a
 976 case study for the Gulf of Guinea. *Ocean Dyn.* 66, 623–636,
 977 <https://doi.org/10.1007/s10236-016-0942-2>.
- 978 Melet A., Meyssignac B. Almar R. et al., 2018. Under-estimated wave contribution to
 979 coastal sea-level rise, *Nature Climate Change*, 8, 234–239, [https://doi.org/10.1007/s10236-](https://doi.org/10.1007/s10236-016-0942-2)
 980 [016-0942-2](https://doi.org/10.1007/s10236-016-0942-2).
- 981 Nerem, R. S. et al., 2018: Climate-change–driven accelerated sea-level rise detected in the
 982 altimeter era. *Proceedings of the National Academy of Sciences*,
 983 <https://doi.org/10.1073/pnas.1717312115>.
 984
- 985 Passaro M., Cipollini P., Vignudelli S. et al., 2014. ALES: A multi-mission subwaveform
 986 retracker for coastal and open ocean altimetry. *Remote Sensing of Environment* 145, 173–189,
 987 <https://doi.org/10.1016/j.rse.2014.02.008>.
- 988 Passaro M., Cipollini P., Benveniste J., 2015, Annual sea level variability of the coastal
 989 ocean: the Baltic Sea-North Sea transition zone. *J Geophys Res Oceans* 120(4):3061–3078,
 990 <https://doi.org/10.1002/2014JC010510>.
- 991 Passaro M., Zulfikar Adlan N. and Quartly G.D., 2018. Improving the precision of sea level
 992 data from satellite altimetry with high-frequency and regional sea state bias corrections.
 993 *Remote Sensing of Environment*, 245–254, <https://doi.org/10.1016/j.rse.2018.09.007>.
- 994 Piecuch C.G., Bittermann K., Kemp A.C. et al., (2018). River-discharge effects on United
 995 States Atlantic and Gulf coast sea-level changes, *PNAS*, vol. 115, no. 30, 7729–7734,
 996 <https://doi.org/10.1073/pnas.1805428115>.
- 997
- 998 Sciascia R., Magaldi M. and Vetrano A., 2019, Current reversal and associated variability
 999 within the Corsica Channel: The 2004 case study, *Deep-Sea Research Part I*, 144, 39–51.
- 1000
- 1001 SROCC 2019: IPCC Special Report on the Ocean and Cryosphere in a Changing Climate
 1002 [H.-O. Pörtner, D.C. Roberts, V. Masson-Delmotte, P. Zhai, M. Tignor, E. Poloczanska, K.
 1003 Mintenbeck, A. Alegría, M. Nicolai, A. Okem, J. Petzold, B. Rama, N.M. Weyer (eds.)].et al.].
 1004 In press.
- 1005 Stammer D, Cazenave A, Ponte RM, Tamisiea ME (2013) Causes for contemporary regional
 1006 sea level changes. *Annu Rev Mar Sci.* <http://doi.org/10.1146/annurev-marine-121211-172406>
 1007
- 1008
- 1009 Wahr, J.M., 1985. Deformation Induced by Polar Motion. *J. Geophys. Res.*, 90 (B11), 9363–
 1010 9368.
- 1011
- 1012 Vignudelli S. , A. G. Kostianoy, P. Cipollini, and J. Benveniste (Eds.), 2011, Coastal
 1013 Altimetry, Springer, Berlin, <https://doi.org/10.1007/978-3-642-12796-0>.
- 1014 The WCRP Global Sea Level Budget Group (2018). Global sea level budget, 1993-present.
 1015 *Earth Syst. Sci. Data*, 10, 1551–1590, <http://doi.org/10.5194/essd-10-1551-2018>.
- 1016 Woodworth P., Melet A., Marcos M. et al., 2019. Forcing Factors Causing Sea Level Changes
 1017 at the Coast, *Surveys in Geophysics*, <https://doi.org/10.1007/s10712-019-09531-1>.

1018

1019 Wöppelmann, G., and M. Marcos (2016), Vertical land motion as a key to understanding sea
1020 level change and variability, *Rev. Geophys.*, 54, 64–92,
1021 <https://doi.org/10.1002/2015RG000502>.